TECHNICAL MEMORANDUM

809

What influences the middle atmosphere circulation in the IFS?

Inna Polichtchouk[1], Robin J. Hogan, Theodore G. Shepherd[1], Peter Bechtold, Tim Stockdale, Sylvie Malardel, Sarah-Jane Lock, Linus Magnusson

Research Department

[1]Department of Meteorology, University of Reading

October 11, 2017

European Centre for Medium-Range Weather Forecasts
Europäisches Zentrum für mittelfristige Wettervorhersage
Centre européen pour les prévisions météorologiques à moyen terme

Series: ECMWF Technical Memoranda

A full list of ECMWF Publications can be found on our web site under:
http://www.ecmwf.int/en/research/publications

Contact: library@ecmwf.int

European Centre for Medium-Range Weather Forecasts
Shinfield Park, Reading, RG2 9AX, England

Abstract

The presence of large ($\sim$ 20 K) middle atmosphere temperature biases motivates an investigation into the representation of the middle atmosphere circulation in the European Centre for Medium-Range Weather Forecasts (ECMWF) Integrated Forecast System (IFS). The focus of this report is on the Brewer-Dobson circulation (BDC) and the zonal-mean temperature and zonal wind structure, and their dependence on: 1) the gravity wave drag parameterizations; 2) the cubic octahedral (TCo) grid and the stochastic physics (SPPT) scheme; 3) the "sponge" in the upper part of the model, designed to prevent wave reflection; and 4) the inclusion of an approximate diurnal cycle of ozone and the reduction of solar UV output. Long free-running model runs are used to assess the performance and sensitivity of the modelled climate. Nudged runs, where the resolved wave fluxes entering the stratosphere are constrained by the observations, are used to assess the model's performance and sensitivity for specific Northern Hemisphere (NH) and Southern Hemisphere (SH) winter conditions. All the results apply to the T255L137 resolution, where a substantial part of the inertia-gravity wave activity is unresolved.

Overall, the parametrized non-orographic gravity wave drag (NOGWD) has the largest impact on the middle atmosphere circulation in all runs. The polar cap downwelling responds to perturbations in NOGWD flux, but there are complex interactions between NOGWD and resolved wave drag in both polar regions in the time-mean and during the seasonal cycle. NOGWD also affects the quasi-biennial oscillation (QBO) and the mesospheric semi-annual oscillation (SAO): The QBO frequency and the QBO and the SAO westerly phase amplitude all increase in response to an increase in the NOGWD, and the SAO easterly phase amplitude decreases in response to a decrease in the NOGWD. The nudging framework allows us to isolate the impact of parametrized orographic gravity wave drag (OGWD) on the polar cap downwelling: NOGWD completely compensates for the removal of OGWD in the NH, but the compensation has an impact on the resolved wave drag.

The TCo grid coupled with the SPPT scheme increases the strength of the lower-stratospheric upwelling and the frequency and westerly phase amplitude of the QBO compared to the control run at the same spectral truncation with linear grid and without SPPT. In the mesosphere, removing the sponge increases the westerly phase of the SAO by 15 times as the resolved waves are allowed to freely propagate into the mesosphere. However, the sponge has no impact on the QBO and little impact on the BDC. The inclusion of the diurnal cycle of ozone and the reduction in solar UV have little impact on the stratospheric circulation despite greatly improving the global warm mesospheric temperature bias.

1 Introduction

Accurate representation of the middle atmosphere circulation in an operational numerical weather prediction model is important for several reasons: i) for tropospheric predictability on medium-range and seasonal timescales, as there is now growing evidence that the stratospheric circulation matters (e.g. Baldwin & Dunkerton 2001, Douville 2009, Sigmond et al. 2013); ii) for getting the correct background information into the data assimilation system, given the deep weighting functions of the operational nadir temperature sounders; and iii) for reanalysis products.

The aim of this report is to assess the state of the middle atmosphere circulation and its dependence on model physics and numerics in the European Centre for Medium-Range Weather Forecasts (ECMWF) Integrated Forecast System (IFS) CY43R1 on seasonal timescales at T255L137 resolution. There are two reasons to believe that the middle atmosphere circulation is inadequately represented in the IFS. Firstly, the free-running model has large ($\sim \pm$20 K) seasonal temperature biases compared to the ERA-Interim (ERA-I) reanalysis (Dee et al. 2011) and to various satellite datasets (see ahead to Figs. 3 and 5). Secondly, in the recent operational analysis (CY43R1) an unphysically strong ($\sim$160 ms^{-1}) westerly

zonal wind develops in the tropical mesosphere at TCo1279 resolution (see ahead to Fig. 23). Therefore, it is of interest to establish if such strong equatorial winds occur in the free-running model at lower resolution. This report focuses on diagnosing the stratospheric Brewer-Dobson circulation (BDC), the semi-annual oscillation (SAO) in the tropical mesosphere, and the quasi-biennial oscillation (QBO) in the stratosphere, in an attempt to understand if the aforementioned model deficiencies result from inadequate representation of these dynamical features in the free-running model.

The BDC is a diabatic mass circulation, with air rising and dynamically cooling in the tropics and descending and dynamically warming in the extra-tropics (see schematic taken from Plumb (2002) in Figure 1). It exerts a crucial control on stratospheric temperature and thereby on winds (e.g., Shepherd 2000). It also plays a key role in the transport of water vapour, ozone and other chemical species. Therefore, inadequate representation of the BDC in the model can lead to large temperature biases.

Rossby and gravity wave breaking and saturation in the middle atmosphere drives the BDC (for a review on the BDC see e.g. Butchart (2014)). In most models, small scale orographic and nonorographic gravity wave breaking and saturation is parametrized (for a review on gravity waves and their parametrization in models see e.g., Fritts & Alexander (2003), Plougonven & Zhang (2014)). From now on the term "NOGWD" will refer to parametrized nonorographic gravity wave drag and "OGWD" to parametrized orographic gravity wave drag. OGWD is an important source of stratospheric drag in both hemispheres in low resolution ($\sim$T42) models (e.g., McLandress & Shepherd 2009, McLandress et al. 2012), with NOGWD playing a lesser role. However, the role of parametrized wave drag should diminish at higher resolution when the wave drag is increasingly resolved by the model. Therefore, the aim of this report is to diagnose the role of the parameterized waves in driving the tropical upwelling and polar cap downwelling at relatively high horizontal resolution in the IFS. The downward control principle of Haynes et al. (1991), which expresses the BDC as a response to breaking and saturating waves aloft, is used to separate the drivers of the BDC into OGWD, NOGWD and the resolved wave drag. Thus far, such a separation has only been carried out for low horizontal resolution (coarser than $1.9\,^{\circ} \times 2.5\,^{\circ}$) stratosphere resolving climate models. Another aim of this report is to assess the interaction of the resolved and parametrized wave drag in the context of a seasonal cycle when parametrized wave drag is altered. So far this has only been addressed in low-resolution climate models (e.g., Sigmond & Shepherd 2014).

The SAO is a twice-yearly oscillation of the zonal-mean zonal wind in the equatorial mesosphere between easterly and westerly phase. The easterly phase maximizes during solstice and is a result of advection across the equator and angular momentum conservation (Meyer 1970). The westerly phase maximizes during equinoxes and is driven by eastward propagating Kelvin and smaller scale gravity waves depositing eastward momentum at the equator (Sato & Dunkerton 1997, Ray et al. 1998). The QBO is an oscillation of equatorial zonal wind in the stratosphere between easterly and westerly phase with a varying period of about 28 months. The phases generally descend with time and are driven by Kelvin waves, mixed Rossby-gravity waves and smaller scale inertia-gravity waves (Dunkerton 1997) that are either resolved or parametrized in the model.

Apart from assessing the middle atmosphere circulation in IFS cycle CY43R1, the sensitivity of the circulation to changes to model physics and numerics, which directly or indirectly affect the momentum budget, is examined. These comprise the already discussed NOGWD and OGWD, and the sponge layer at the model top. Recent changes to the spectral dynamical core include the computation of the nonlinear terms on a reduced cubic octahedral grid (TCo grid) (Malardel et al. 2016) instead of the linear Gaussian grid (TL grid) . The TCo grid de-aliases triad interactions by representing the shortest wave by four rather than two grid points, thus doubling the horizontal physical-space resolution compared to the TL grid at the same spectral truncation. The reduction of aliasing with the TCo grid allows for a better filtered representation of orography and less numerical diffusion in the dynamical core. To generate

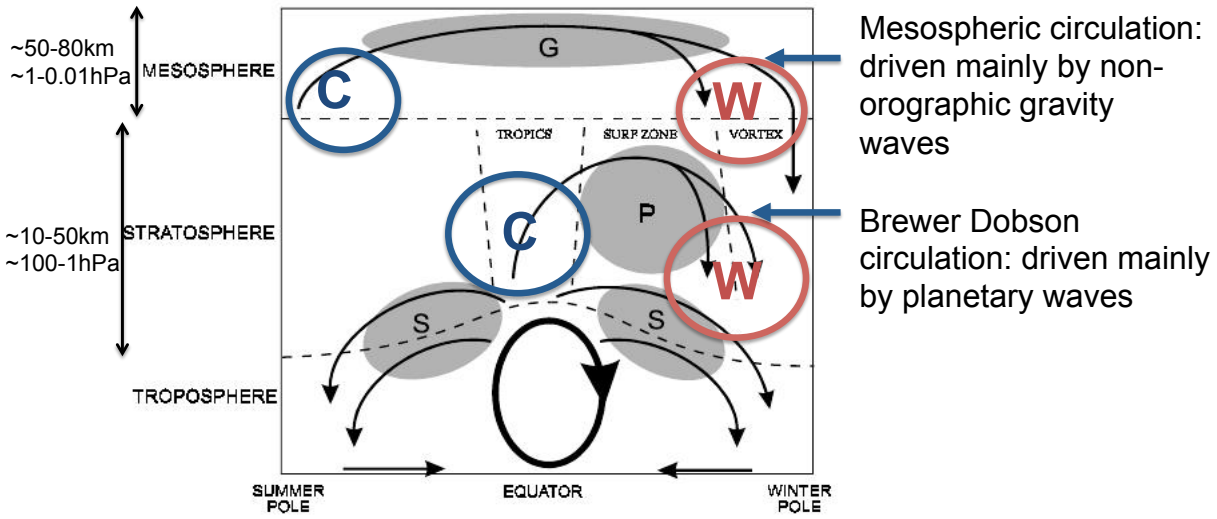

Figure 1: Schematic of the residual mean meridional circulation taken from Plumb (2002): The heavy ellipse denotes the thermally-driven tropospheric Hadley cell. The shading denotes regions of wave breaking responsible for driving the middle atmosphere circulation. "S" stands for synoptic waves, "P" for planetary waves, and "G" for gravity waves. Ascent induces adiabatic cooling denoted by "C" and descent adiabatic warming denoted by "W".

ensemble spread in the ensemble prediction system (ENS), a stochastic physics scheme (SPPT) is used, in which the tendencies from the physics parametrization are perturbed with synoptic-scale noise that is correlated in time (Palmer et al. 2009). Thus, it is of interest to examine the sensitivity of the middle atmosphere circulation to the use of the TCo grid coupled with the SPPT scheme. Recent work in ECMWF (2017) shows how the inclusion of an approximate diurnal cycle of ozone and the reduction in solar UV output in the radiation scheme in the IFS has a potential for substantially reducing the large global-mean warm biases in the mesosphere. Therefore it is also of interest to establish whether improvements in the mesospheric temperatures impact the BDC or the SAO and the QBO.

The report is organized as follows. Section 2 reviews the experimental setups, the diagnostics, and the data sets used to evaluate the model runs. To motivate the sensitivity experiments, section 3 presents the zonal momentum budget for the control IFS experiment. In section 4, the temperature distribution from the control experiments under both setups is compared to the observational data sets. In this section the effect of model changes on the temperature and zonal wind distribution is also discussed. In section 5, the tropical water vapour tape recorder signal, used as a proxy for tropical upwelling, is first diagnosed in the free-running model and compared to the tape recorder signal in observations. The residual mean meridional circulation, split into its resolved and parameterized wave drivers, is then diagnosed in the model and the impact of model changes — especially on the downwelling over the polar caps — is discussed. Section 6 evaluates the representation of the QBO and SAO in the model and how it depends on model numerics. Finally, conclusions are given in section 7.

2 Method

2.1 Model description and setup

The IFS is a global semi-Lagrangian spectral model developed and used for operational forecasts. The detailed description of its dynamical core and the physical parameterizations — as used in cycle CY43R1— can be found in ECMWF (2016). Here, the IFS is run at T255 spectral truncation[1] with both the TL grid (grid spacing of ∼80 km) and the TCo grid (grid spacing of ∼40 km). The vertical domain is resolved by 137 levels (at 100 hPa the vertical resolution is ∼300 m, coarsening to ∼1.5 km at 1 hPa) and the model top is located at 0.01 hPa. To prevent wave reflection at the model top, a fourth order hyper-diffusion (∇^4) is applied on vorticity, divergence and temperature above 10 hPa to damp vertically propagating waves. The hyper-diffusion *e*-folding timescale on the largest resolved wavenumber varies with altitude from 0.65h at 10 hPa to 0.03h at the model top. In addition, a first order damping (∇) is applied on divergence only above 1 hPa with the *e*-folding timescale on the largest resolved wavenumber decreasing from 0.1h at 1 hPa to 0.02h at the top of the model. Both "sponges" damp the zonal-mean flow (i.e., apply diffusion on the zonal wavenumber $m = 0$ coefficients, but not on the total wavenumber $n = 0$ coefficients).

The NOGWD parameterization in the IFS follows Scinocca (2003). Orr et al. (2010) discuss in detail the specific implementation and beneficial effect of this parametrization on the middle atmosphere circulation in the IFS. In the default setting, the momentum source is represented by a broad spectrum of wave speeds (half-width of 150 ms^{-1}) discretized into 25 variable resolution phase speed bins and launched at 450 hPa[2]. The amplitude of the launch spectrum is 3.75 mPa, with a reduction in amplitude to 75% in the tropics[3]. The OGWD parameterization in the IFS follows Lott & Miller (1997).

To assess the state of the middle atmosphere circulation in the IFS at T255L137 resolution, two different experimental protocols are followed: 1) an ensemble of four-year forecasts spanning eleven years of observational Microwave Limb Sounder (MLS) data; and 2) nudged forecasts spanning one winter and spring season, in which the troposphere below 500 hPa is relaxed to the ERA-I reanalysis. In both types of experiments, the observed sea-surface temperatures are prescribed. The "free-running" setup 1 allows us to study the response of model's climatology to model changes. Setup 2 allows us to study the response of internal middle atmosphere dynamics to model changes and to reproduce specific winter events (e.g., stratospheric sudden warmings (SSWs)).

In setup 1, eight four-year forecasts are initialized one year apart starting from 01/08/2004. The first month is disregarded as spin-up. This procedure samples the 11-year time period from 2004 to 2015 and generates 32 (non-independent) years of data. The control simulation is integrated on a TL grid with all the default parameterization specifications for cycle 43R1. To study the effect of NOGWD on the middle atmosphere circulation, the amplitude of the launch spectrum is reduced to 1 mPa in one simulation and increased to 14 mPa in another. The launch amplitudes are within the observed range of absolute gravity wave momentum fluxes in the lower stratosphere (see e.g., Fig 1 in Geller et al. 2013). Moreover, using the data-assimilation technique Scheffler & Pulido (2017) showed that the SH optimal launch momentum flux can fluctuate between three to 0.5 times the reference value over the seasonal cycle. To study the effect of the TCo grid with the SPPT scheme, these options are enabled in the fourth simulation. As the

[1] With the exception of nudged runs with the TCo grid, which are performed at T319 truncation. This is due to the unavailability of the nudging dataset at TCo255 resolution.

[2] The 450 hPa launch level implies that NOGWs can break in the upper troposphere and lower stratosphere on encountering critical levels, such as when the subtropical jets terminate in the equatorial lower stratosphere.

[3] Note that this setup is appropriate for the seasonal prediction system with the TCo grid and SPPT scheme switched on. In the operational SEAS5, which has 91 levels, the launch spectrum is reduced in amplitude to 25% in the tropics, something not replicated in this experiment.

Table 1: List of experiments for the free-running setup 1. Note that only temperature and zonal winds are output in the "no sponge" run. The forecasts are initialized one year apart, starting from 01/08/2004.

Name of run	Resolution	Length of run	NOGWD flux [mPa]	SPPT	Sponge
Control	TL255L137	8 × four-years	3.75	Off	On
Reduced NOGWD	TL255L137	8 × four-years	1	Off	On
Increased NOGWD	TL255L137	8 × four-years	14	Off	On
TCo+SPPT	TCo255L137	8 × four-years	3.75	On	On
No sponge	TL255L137	8 × four-years	3.75	Off	Off

Table 2: List of experiments for the nudged setup 2. The vorticity and temperature fields in the troposphere, below 500 hPa, are nudged to the ERA-I. One set of forecasts is initialized on 01/11/2005 and another on 01/05/2006.

Name of run	Resolution	Length of run	NOGWD flux [mPa]	SPPT	OGWD	ensemble size
Control	TL255L137	2 x seven months	3.75	Off	On	5
Reduced NOGWD	TL255L137	2 x seven months	1	Off	On	5
Increased NOGWD	TL255L137	2 x seven months	14	Off	On	5
TCo+SPPT	TCo319L137	2 x seven months	3.75	On	On	5
No sponge	TL255L137	2 x seven months	3.75	Off	On	5
No OGWD	TL255L137	2 x seven months	3.75	Off	Off	5
UV, O_3 + no sponge	TL255L137	2 x seven months	3.75	Off	On	5

TCo grid and SPPT are used in the ensemble prediction system at ECMWF, it is important to evaluate the effect of both these options on the model's climatology. The effect of the sponge on the middle atmosphere temperature structure is also studied by removing the sponge.

In the nudged setup 2, the relative vorticity and temperature fields are relaxed via Newtonian relaxation to the ERA-I reanalysis on the terrain-following model levels below 500 hPa. The fields up to total wavenumber 61 in the spherical harmonic expansion are nudged. The relaxation timescale for relative vorticity is 12 h and for temperature 5 days. The nudging approach isolates the role of internal stratospheric dynamics as the wave forcing from the troposphere is not affected by model changes. This allows for a clean separation of cause and effect. As the nudging approach eliminates internal tropospheric variability, long runs are not required. Two seven-month forecasts are performed for the NH winter and spring 2005/2006 that experienced a long-lived SSW event, and for the SH winter and spring 2006. In addition to NOGWD flux and the TCo grid and the SPPT scheme, the nudged setup is also used to study the model's response to the absence of a sponge and the inclusion of the diurnal cycle of ozone (O_3) and the decreased solar UV output in the radiation scheme. The nudged setup also allows us to study the impact of removing parametrized OGWD on the middle atmosphere circulation as the removal of OGWD would adversely impact the tropospheric circulation in the free-running model.

As noted in Seviour et al. (2012) and Sakazaki et al. (2015) there is a strong diurnal cycle in the zonal mean fields in the stratosphere – especially in the tropics – that is associated with thermal tides and convection. Therefore, all the fields are output every 6h to sample the diurnal cycle.

2.2 Evaluation data sets

To validate the control runs under both setups, version 3.3 of the temperature and specific humidity data from the MLS instrument (Livesey et al. 2011) on-board the *Aura* satellite is used. MLS has provided continuous observations of the middle atmosphere from September 2004 to the present day and is used here for evaluation between September 2004 and September 2014. The useful pressure range for the temperature observations is 261–0.001 hPa and for specific humidity observations 316-0.002 hPa. The vertical resolution of the MLS data is 5 km. Model output is linearly interpolated to MLS resolution when evaluating the model against MLS.

The runs are also validated against ERA-I temperature, zonal wind and specific humidity reanalysis. Note that ERA-I reanalysis is only available at heights below 0.1 hPa. Additionally, the model used in ERA-I has a sponge layer above 10 hPa and is unconstrained in the mesosphere by the observations. Therefore, this region of ERA-I data should not be regarded as "truth", as all the model biases come through in the reanalysis.

2.3 Diagnostics

The Transformed Eulerian Mean framework is used to diagnose the residual mean meridional circulation (Andrews et al. 1987). The residual mean mass streamfunction Ψ is:

$$\Psi \equiv -\frac{\cos\phi}{g}\int_p^0 \overline{v}^*(\phi,p')dp', \tag{1}$$

where the residual meridional wind $\overline{v}^*$ is

$$\overline{v}^* = \overline{v} - \frac{\partial}{\partial p}\left(\frac{\overline{v'\theta'}}{\partial\overline{\theta}/\partial p}\right) \tag{2}$$

and $\overline{(.)}$ denotes the zonal-mean and $()'$ the deviation of a field from the zonal-mean, v is meridional wind, θ is potential temperature, p is pressure, ϕ latitude, g gravitational acceleration, and at $p=0$, $\Psi=0$ is imposed.

To diagnose the contributions of OGWD and NOGWD (recall these refer to the parametrized waves) and the resolved wave drag in driving the BDC, the downward control principle of Haynes et al. (1991) is used. It expresses the steady residual mean meridional circulation as a response to drag from breaking/saturating waves aloft.

The downward control streamfunction Ψ_{DC} is:

$$\Psi_{\mathrm{DC}} \equiv \frac{\cos\phi}{g}\int_p^0 \frac{\overline{D}(\phi,p')}{f-(a\cos\phi)^{-1}\partial(\overline{u}\cos\phi)/\partial\phi}dp', \tag{3}$$

where a is the Earth's radius, f is the Coriolis parameter, u is the zonal wind, and $\overline{D}$ is the zonal-mean wave drag composed of the tendency terms in the zonal momentum equation due to the resolved wave drag and NOGWD and OGWD. Resolved wave drag is given by $\nabla\cdot\mathbf{F}/a\cos\phi$, where $\mathbf{F}$ is the Eliassen-Palm (EP) flux

$$\mathbf{F} = \{F_\phi, F_p\} = a\cos\phi\left(\frac{\overline{\theta'v'}\partial\overline{u}/\partial p}{\partial\overline{\theta}/\partial p} - \overline{u'v'}, \frac{\overline{\theta'v'}}{\partial\overline{\theta}/\partial p}(f-\frac{1}{a\cos\phi}\frac{\partial\overline{u}\cos\phi}{\partial\phi}) - \overline{u'\omega'}\right), \tag{4}$$

where ω is the vertical "pressure" velocity. The residual vertical velocity $\overline{w}^*$ is computed following McLandress & Shepherd (2009):

$$\overline{w}^* = \frac{gH}{pa\cos\phi}\frac{\partial\Psi}{\partial\phi}, \tag{5}$$

where H is the pressure scale height $H = 7$ km. Similarly, $\overline{w}^*_{\mathrm{DC}}$ can be calculated from Ψ_{DC}.

The vertical mass flux across a pressure surface poleward of latitude ϕ in the NH and SH is given by Holton (1990):

$$F_{\mathrm{NH}} = 2\pi a^2\rho\int_{\phi}^{\pi/2}\overline{w}^*\cos\phi d\phi \tag{6}$$

and

$$F_{\mathrm{SH}} = 2\pi a^2\rho\int_{-\pi/2}^{\phi}\overline{w}^*\cos\phi d\phi, \tag{7}$$

where ρ is density. Instead of evaluating the integral in (3) on constant angular momentum contours, it is evaluated at a constant latitude. This is a good approximation outside the tropics. Expressed in terms of Ψ and noting that Ψ vanishes at the poles, the downward mass flux poleward of latitude ϕ is given by $F_{\mathrm{NH}} = 2\pi a\Psi(\phi)$ and $F_{\mathrm{SH}} = -2\pi a\Psi(\phi)$. The upward tropical mass flux between two latitudes ϕ and $-\phi$ is given by $F_{\mathrm{TR}} = 2\pi a\{\Psi(\phi) - \Psi(-\phi)\}$. F_{TR} is calculated between the 'turnaround' latitudes as in McLandress & Shepherd (2009), Butchart et al. (2011). The turnaround latitudes are located between the minimum and maximum values of Ψ (i.e., where the tropical upwelling changes to extra-tropical downwelling). Similarly, using the downward control streamfunction $F_{\mathrm{NH}} = 2\pi a\Psi_{\mathrm{DC}}(\phi)$, $F_{\mathrm{SH}} = -2\pi a\Psi_{\mathrm{DC}}(\phi)$, and $F_{\mathrm{TR}} = 2\pi a\{\Psi_{\mathrm{DC}}(\phi) - \Psi_{\mathrm{DC}}(-\phi)\}$.

3 Zonal momentum budget in the control run

Before diagnosing the BDC, it is useful to document the distribution of parametrized and resolved wave drag in the middle atmosphere for this version of the IFS. The momentum budget for the IFS at TL159L91 resolution has been diagnosed and discussed for July and December in Orr et al. (2010). It is shown here for different seasons for the control integration in Fig. 2. The key features are:

- All waves act to decelerate the zonal-mean zonal wind in the extra-tropics.
- The resolved planetary waves (left column) and stationary parametrized OGWs (right column) can propagate and break/saturate in the middle atmosphere when the background zonal winds are westerly. Zonal wavenumber decomposition shows that most of the resolved wave drag is coming from wavenumbers one to three (not shown). This is true even in the mesosphere as the strong sponge applied above 1 hPa is very effective in damping the higher-frequency smaller-scale resolved waves. The resolved wave drag is stronger in the NH, where it attains its maximum in mid-winter. In the SH, the resolved wave drag attains its maximum in late winter/spring. This temporal asymmetry is consistent with observations (e.g., Randel 1988, Quintanar & Mechoso 1995) and the theory of Charney & Drazin (1961), which states that planetary waves can propagate into the middle atmosphere when the background westerlies are less than a threshold value. This value is generally less than the SH mid-winter westerly wind speed.
- In the tropical lower-stratosphere, the resolved wave drag consists mostly of synoptic and transient planetary wave breaking on the equatorward flank of the subtropical jet. These waves break throughout the year and are important for driving the tropical upwelling (Randel et al. 2008).

- NOGWs (middle column) are filtered by the background zonal wind: The westward propagating waves are filtered by the easterlies and the eastward propagating waves by the westerlies (e.g., Shepherd 2000) leading to eastward drag and polar ascent in the summer mesosphere and westward drag and polar descent in the winter mesosphere. In the summer hemisphere, NOGWD dominates the mesospheric drag as the resolved gravity waves are damped by the strong sponge.
- NOGWD is largest in the SH, where it is the dominant parametrized wave forcing, because of stronger preferential filtering of eastward vs westward propagating waves. In contrast to what is found in lower-resolution models, OGWD is only stronger than NOGWD during the NH winter in the lower mesosphere. The integrand in (3) is density weighted, so the waves exerting drag at altitudes further above the stratosphere have less impact on the BDC. Given the above, the effect of the NOGWD flux changes on the BDC, and in particular on the downwelling over the pole, is expected to be smaller in the NH winter than in the SH winter.

4 Temperature and zonal wind distributions

4.1 Temperature and zonal wind bias

Figure 3 shows the zonal-mean temperature ($\overline{T}$) bias with respect to MLS (top) and ERA-I (bottom) for the control run with setup 1 for DJF and JJA, respectively. Figure 4 shows the zonal-mean zonal wind ($\overline{u}$) bias against ERA-I. Note that the ERA-I comparison is only shown up to 0.1 hPa. Compared to both datasets, the model has a clear SH winter upper-stratospheric (10-1 hPa) warm bias of $\sim$10 K centered at $\sim$ 55 °S that might be due to too strong a downwelling at the edge of the polar vortex. Moreover, there is a cold tropical lower-stratosphere (100-10 hPa) bias of $\sim$3 K when compared to ERA-I that could be suggestive of too strong an ascent and dynamical cooling. The reason why this bias is not showing up when compared to the MLS data might be due to too coarse a vertical resolution in the MLS data near the tropopause (5 km). Therefore ERA-I is probably a better data set to evaluate the model against in the vicinity of the tropopause.

Overall, the upper stratosphere appears to be biased warm compared to both datasets. In the SH winter, the IFS exhibits the common model bias of the polar night jet not having enough equatorward tilt at the stratopause. At the polar tropopause, a cold bias of $\sim$5 K, which maximizes in the summer hemisphere, is present. Again this bias is more pronounced in comparison to ERA-I. The bias is longstanding and is common to almost all climate models (Boer et al. 1992), (Chapter 4 in *SPARC CCMVal Report on the Evaluation of Chemistry-Climate Models* 2010). The bias results in the subtropical jets being shifted poleward compared to ERA-I in the upper troposphere/lower stratosphere (see Fig. 4). This bias might be related to too much moisture "leakage" from the troposphere to the stratosphere by the semi-Lagrangian scheme (Diamantakis 2013) resulting in too much longwave cooling. In low resolution models, this bias is somewhat reduced by increased vertical resolution, removal of the quasi-monotone filter, the higher order semi-Lagrangian interpolation (e.g. Diamantakis 2013, Pope et al. 2001), the move from Eulerian to semi-Lagrangian dynamics (Mike Blackburn, personal communication), and the use of isentropic coordinates in the stratosphere (Chen & Rasch 2012).

In the mesosphere, the model is biased warm by $\sim$20 K, with the largest bias occurring in the summer hemisphere. As has already been discussed in ECMWF (2017) and as will be shown below, this bias is largely eliminated by the introduction of the diurnal cycle in ozone and the decrease in the solar UV output. It should be emphasized that the ERA-I zonal winds in the mesosphere should not be regarded as truth because the mesosphere feels the strong sponge in ERA-I.

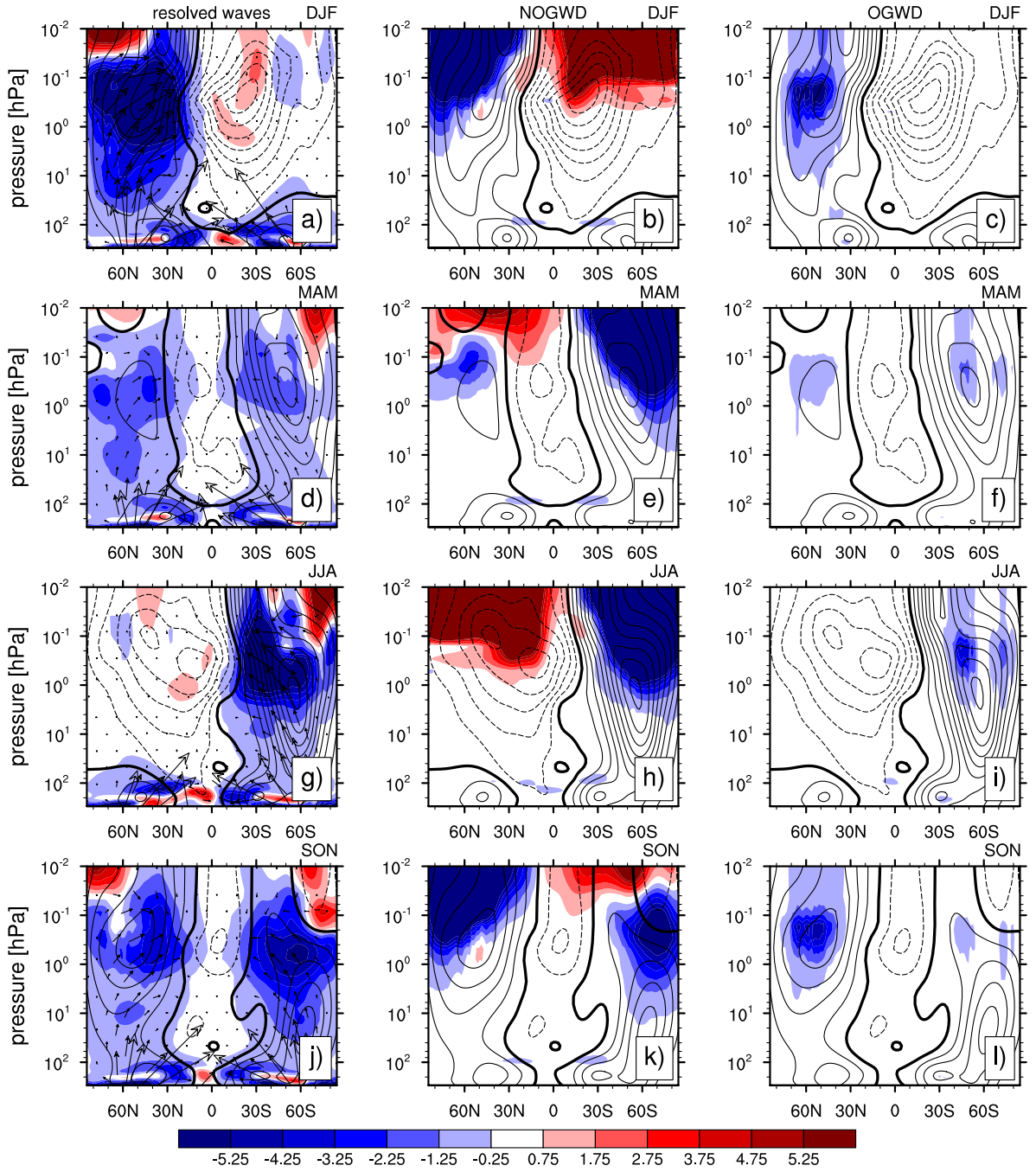

Figure 2: Latitude-pressure cross sections of zonal-mean zonal momentum tendencies in m s^{-1} day^{-1} for the control run in the middle atmosphere: (a,b,c) December-February (DJF), (d,e,f) March-May (MAM), (g,h,i) June-August (JJA), and (j,k,l) September-November (SON). First column: Resolved wave tendency. The EP flux vectors are represented by the arrows (in m^3 s^{-2}). Second column: NOGWD tendency. Third column: OGWD tendency. Negative values are shaded in blue and positive in red. The contour interval for wave tendencies is 1 m s^{-1} day^{-1}. The zonal-mean zonal wind, in m s^{-1}, is shown in black contours (contour interval 10 m s^{-1}), negative contours are dashed and the zero contour is drawn with double thickness.

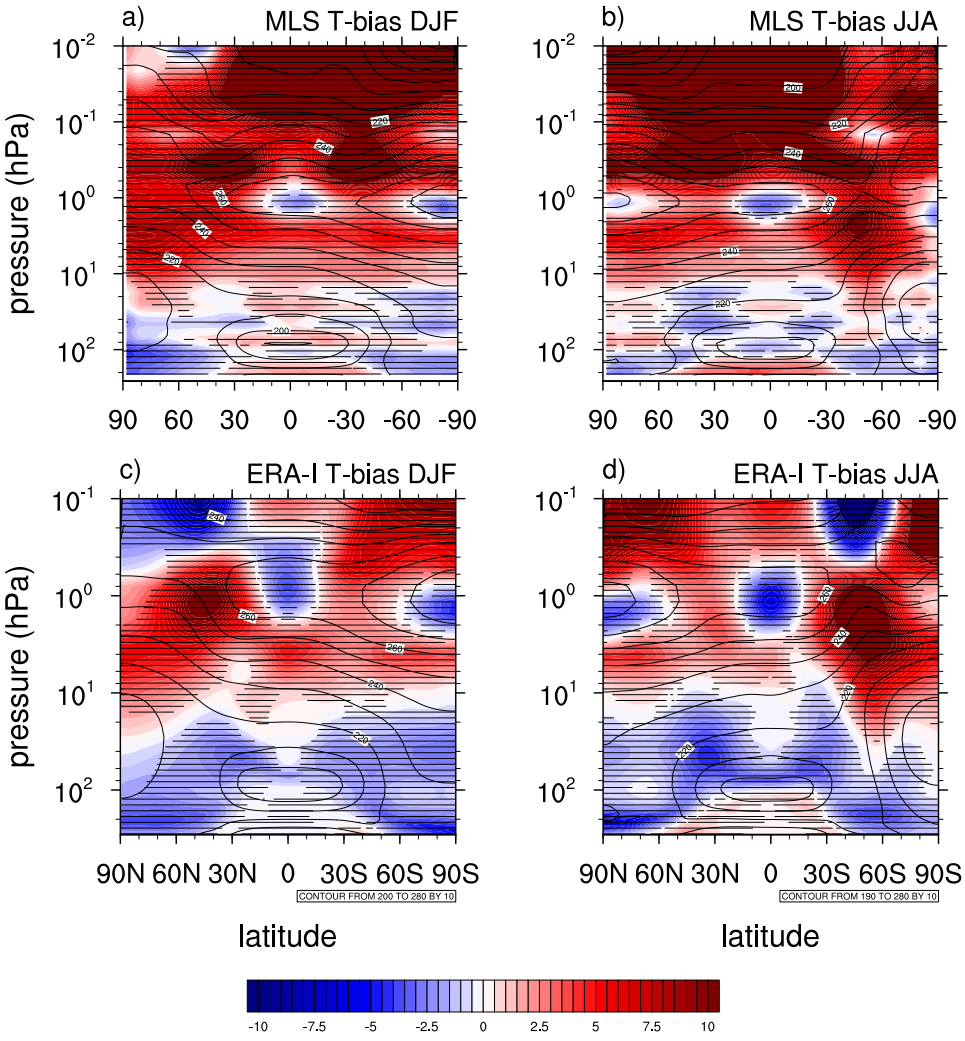

Figure 3: Latitude-pressure cross section of $\overline{T}$ bias for setup 1 for DJF and JJA against (a and b) MLS and (c and d) ERA-I. The black contours show the observation and reanalysis climatologies. The stippling shows where the dataset and model climatologies are different at the 95% significance level by the Student t-test on the means. Note the different vertical ranges between the top and bottom panels.

Figure 5 shows the $\overline{T}$ bias and Fig. 6 shows the $\overline{u}$ bias for the control run with the nudged setup 2. The biases in the nudged setup are nearly identical to the biases in the free-running model in JJA in both hemispheres and in DJF in the summer hemisphere only. The similarity of the biases implies that they are not related to the representation of tropospheric wave sources. Because of its cheapness to run and analyze, this makes the nudged setup attractive in trying to understand and resolve these seasonal $\overline{T}$ biases. The NH winter is too variable from year to year and the nudged setup that only runs for one winter does not capture the $\overline{T}$ and $\overline{u}$ bias statistics from the 32-year run with the free-running model. It should be noted that sub-sampling four years from a total of 32 years in setup 1 also reproduces the $\overline{T}$ bias in JJA in both hemispheres and in DJF in the summer hemisphere only. Therefore even one four-year forecast is enough to capture these $\overline{T}$ biases.

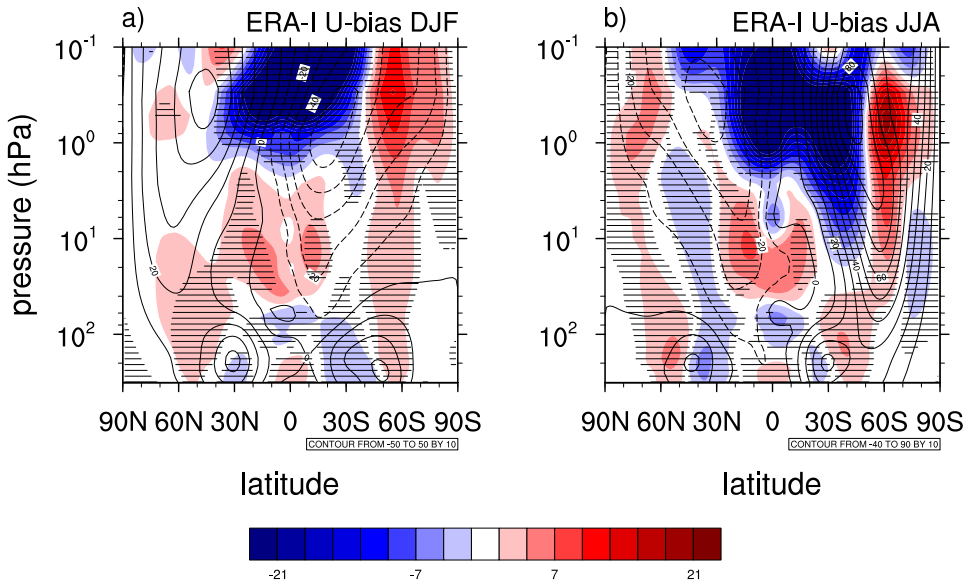

Figure 4: Latitude-pressure cross section of $\overline{u}$ bias for setup 1 against ERA-I for (a) DJF and (b) JJA. The black contours show the ERA-I climatology. The stippling shows where the ERA-I and model climatologies are different at the 95% significance level by the Student t-test on the means.

4.2 Impact of model changes on temperature and zonal wind distributions

4.2.1 Non-orographic gravity wave drag

The effect of NOGWD parametrization on the middle atmosphere $\overline{T}$ and $\overline{u}$ distributions in the IFS has been extensively studied in Orr et al. (2010) at TL159L60 resolution. Figures 7–8 show $\overline{T}$ and $\overline{u}$ responses to reduction and increase of the parametrized NOGWD flux by 3.75 times in the free-running setup. It is clear from the figures that NOGWD plays a major role in the $\overline{T}$ and $\overline{u}$ distributions in the middle atmosphere. In particular, reducing NOGWD leads to acceleration of the zonal winds aloft, dynamical warming over the summer pole and cooling over the winter pole. This is expected since NOGWD acts to decelerate zonal winds in the middle atmosphere in the extra-tropics. Therefore, reducing NOGWD allows the winds to become stronger than in the control run. The warming over the summer pole and cooling over the winter pole are consistent with less NOGWD induced upwelling and downwelling, respectively. Recall that eastward propagating NOGWs can enter the middle atmosphere in the summer, when the stratospheric zonal winds are easterly. When the eastward propagating waves saturate, they induce positive momentum flux convergence over the summer poles and therefore upwelling and adiabatic cooling. The westward propagating NOGWs can enter the middle atmosphere mostly in winter, when the stratospheric zonal winds are westerly. When the westward propagating waves saturate, they induce negative momentum flux convergence over the winter poles and therefore downwelling and adiabatic warming. The $\overline{T}$ response is opposite when the NOGWD flux is increased. Note that the dynamical warming/cooling in the winter hemisphere extends lower into the stratosphere in the SH compared to the NH. This is consistent with the diagnostics in Fig. 2 that show the deeper (and stronger) influence of NOGWD on the momentum budget in the SH winter compared to the NH winter. The cooling/warming in the summer hemisphere is similar in both hemispheres.

The $\overline{T}$ and $\overline{u}$ response in the nudged setup 2 is almost identical to the response in the free-running model in JJA and in DJF in the summer hemisphere only. This can be seen in Fig. 9 for the case of

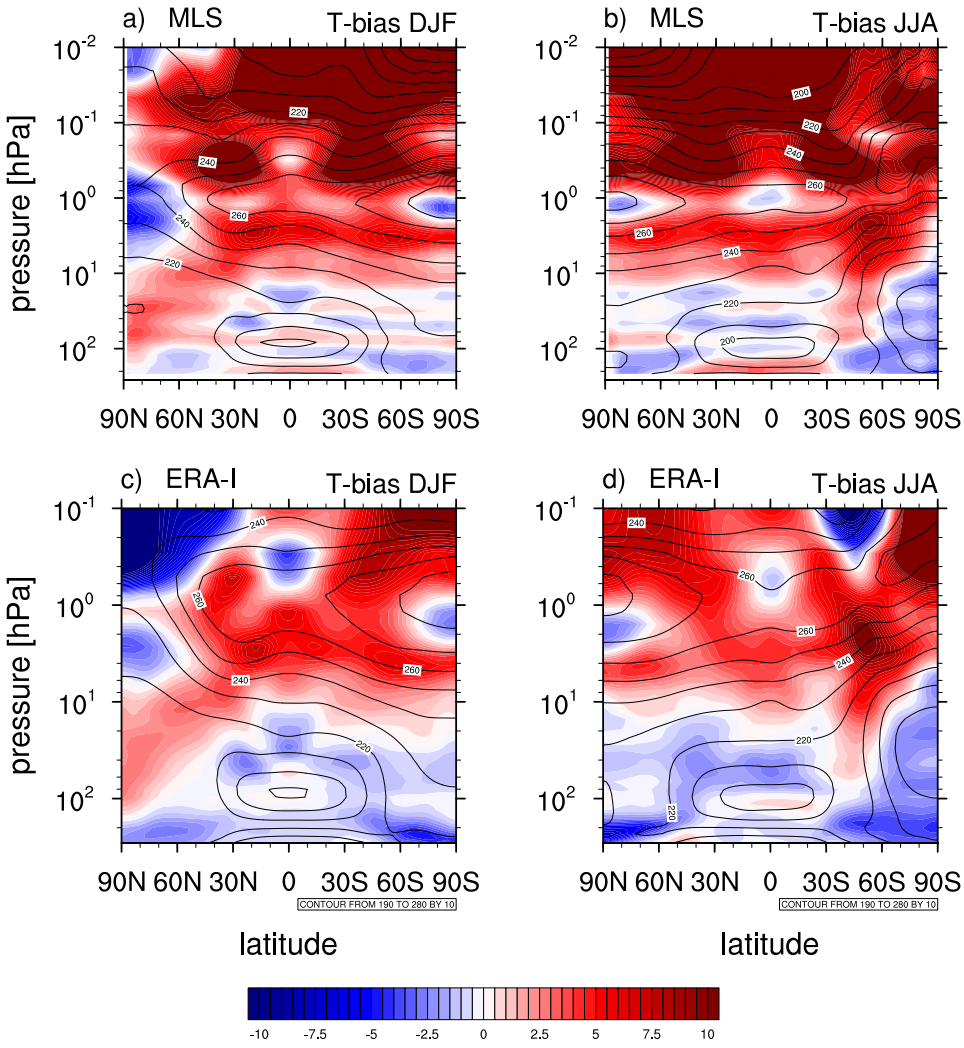

Figure 5: Same as Fig. 3 but for the nudged setup 2. Note that the bias is calculated for year 2005/2006 in DJF and for year 2006 in JJA.

reduced NOGWD. This is also the case when sub-sampling four years from a total of 32 years in the free-running setup 1. Therefore one four-year forecast is enough to establish the sensitivity to NOGWD flux in summer hemispheres and in the SH winter.

Note that the $\overline{T}$ response over the SH winter pole to changes in NOGWD is deep and extends all the way through the stratosphere. The deep response is not expected from the distribution of NOGWD, which peaks in the mesosphere (see Fig. 2). The deep response indicates that the resolved waves are strongly involved in the response. This will be discussed further in section 5. Because of the deep response, reducing NOGWD can not address the persistent warm $\overline{T}$-bias in the SH winter upper-stratosphere (see Fig. 3), which is a shallow feature. Moreover, given the asymmetric $\overline{T}$-response in the mesosphere (e.g., warming in the summer mesosphere and cooling in the winter mesosphere in response to reduced NOGWD), NOGWD changes will not improve the global warm bias in the mesosphere. NOGWD changes are also not likely to improve the lower stratospheric tropical cold bias as the impact of NOGWD changes on the tropical lower-stratospheric temperatures is small. Overall, the current NOGWD settings seem to be optimal for $\overline{T}$ and $\overline{u}$ distributions at T255L137 resolution.

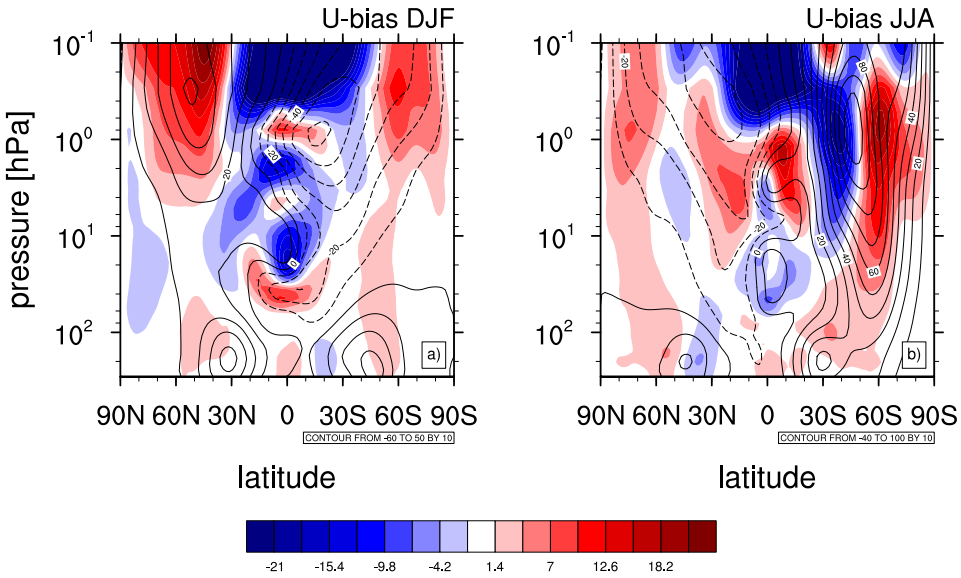

Figure 6: Same as Fig. 4 but for setup 2. Note that the bias is calculated for year 2005/2006 in DJF and for year 2006 in JJA.

4.2.2 TCo grid and SPPT

Figure 10 shows the $\overline{T}$ and $\overline{u}$ response to the use of the TCo grid at T255 spectral truncation coupled to the SPPT scheme (TCo+SPPT). In the tropical lower stratosphere and in the summer stratosphere, there is a robust $\sim 1-2$ K cooling in response to TCo+SPPT in both setups (the nudged setup is not shown). It should be noted that a similar cooling is also seen in the TCo399 run, without SPPT switched on, when compared to the TL255 run. The $\overline{u}$ response to TCo+SPPT in the nudged runs is also robust in the tropics. In mid-latitudes, however, the nudged setup 2 does not reproduce the winter $\overline{T}$ response of the free-running setup 1 (not shown). This indicates either that the response to TCo+SPPT is not robust and very sensitive to the basic state or that the response in the free-running model comes from the effect of TCo+SPPT on the wave forcing in the troposphere (for total wave numbers smaller than 61), as the nudged setup constrains the wave forcing to ERA-I below 500 hPa. Moreover, sub-sampling four-year responses from setup 1 shows a range of $\overline{T}$ responses in winter mid-latitudes, indicating that using one four-year forecast is not enough to establish the impact of TCo+SPPT on the middle atmosphere mid-latitude circulation.

4.2.3 The sponge

A sponge applied on the zonal-mean flow (i.e., the zonal wavenumber $m = 0$ mode in the spherical harmonic expansion) can lead to coupling to the lower-level dynamics in an artificial manner and result in an unrealistic response to forcing (Shepherd et al. 1996). Moreover, the amplitude of both divergent and rotational modes in the stratosphere increases with horizontal resolution and an increasingly resolved spectrum of inertia gravity waves. As a result, applying a sponge that acts differently on divergence and vorticity may have substantial and unwanted side effects. Therefore, an equal-strength sponge should be applied on the vorticity and divergence fields in the mesosphere. Such a sponge is currently under development. To study the effect of the default sponge on the middle atmosphere circulation in the current model version, the sponge is removed altogether.

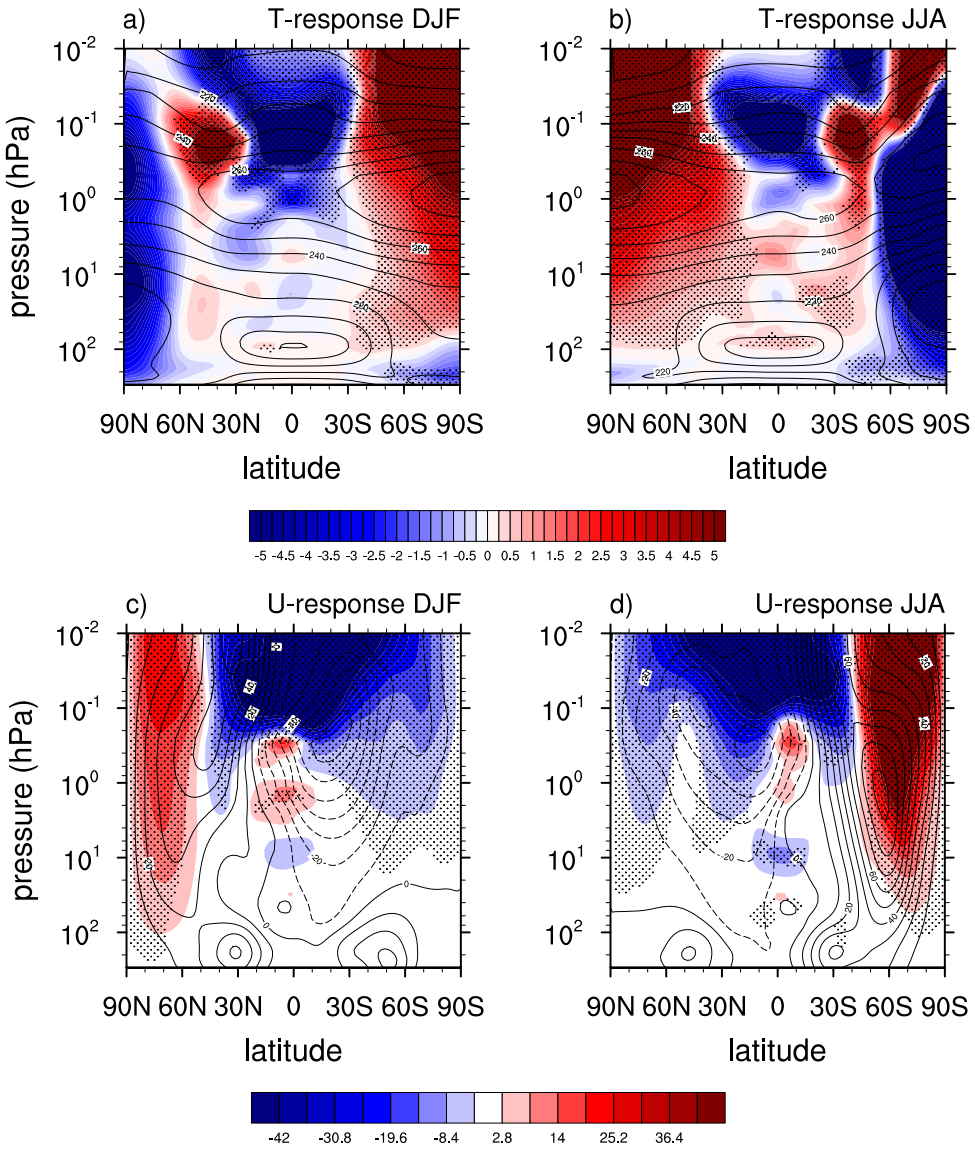

Figure 7: Latitude-pressure cross section of (a-b) $\overline{T}$ response (i.e. perturbation experiment minus control) and (c-d) $\overline{u}$ response to reduction in NOGWD flux for DJF and JJA for the free-running setup. The stippling shows where the model climatologies are different at the 95% significance level by the Student t-test on the means.

Figure 11 shows the $\overline{T}$ and $\overline{u}$ responses to the removal of the sponge. The effect of removing the sponge is to cool the global-mean mesosphere by ∼5 K. Hence, the absence of the sponge may improve the warm $\overline{T}$ bias in the mesosphere. The cooling mostly occurs over the summer poles. However, the absence of a sponge warms the winter poles. An additional experiment, in which the extra sponge on the divergence field was removed, produces an almost identical response to the "no sponge" case (not shown). This suggests that the summer hemisphere cooling response and the winter polar warming response is tied with the resolved gravity wave activity: The absence of a sponge on the divergence field allows more resolved gravity waves to enter the mesosphere and induce more upwelling in the summer hemisphere and downwelling in the winter hemisphere.

The winter hemisphere $\overline{T}$ response to no sponge in the free-running runs produces a quadrupole pattern

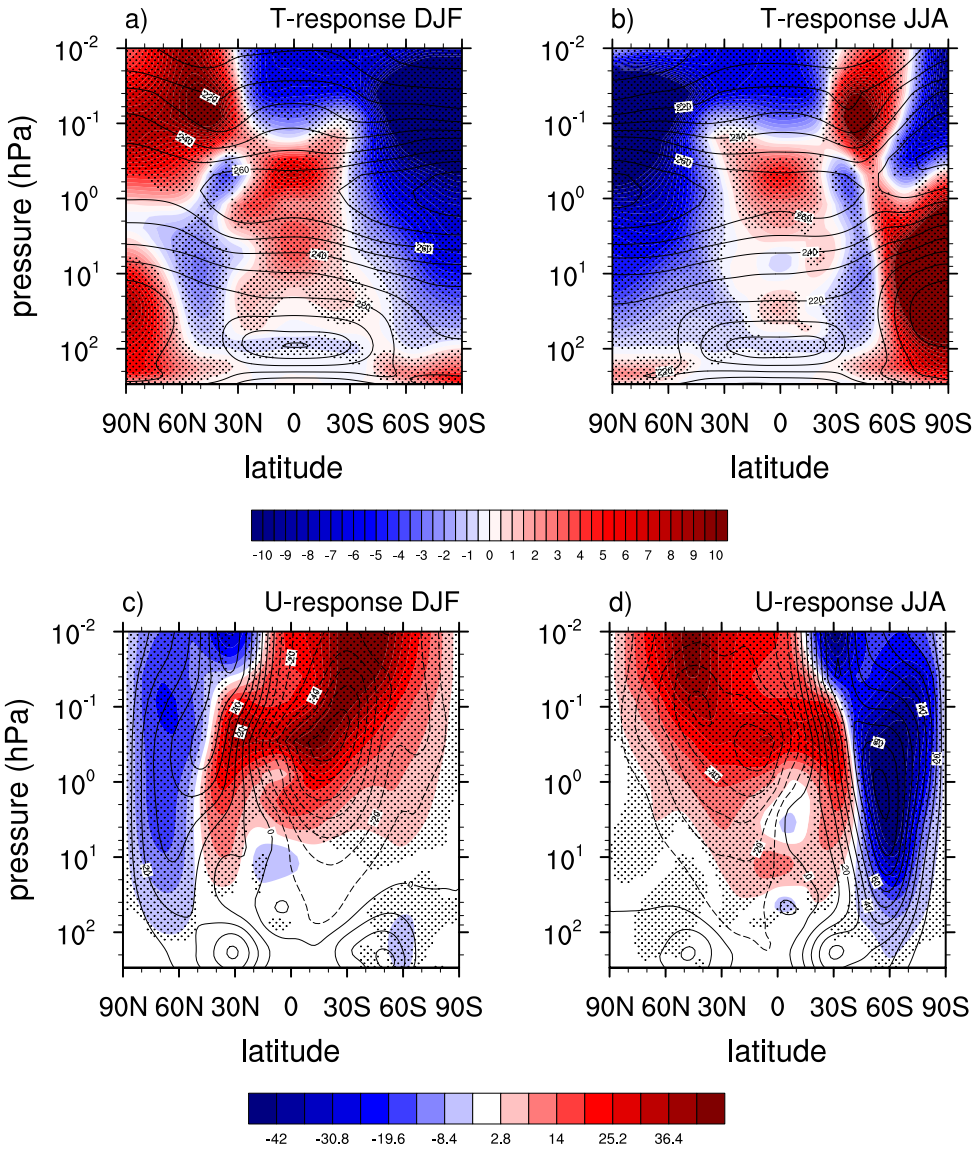

Figure 8: Same as Fig. 7 but for response to increase in NOGWD flux.

above 5 hPa in Fig. 11. This quadrupole response is very similar to Fig. 3 in Shepherd et al. (1996), who find that a negative momentum force (such as wave drag from the resolved waves) applied inside the sponge that damps the zonal-mean flow produces a quadrupole response when compared to the run without a sponge on the zonal-mean flow. This quadrupole response is robust and is there when sub-sampling four years from setup 1. Note that in the SH winter, the removal of the sponge in the free-running setup appears to alleviate the stratospheric mid- to high-latitude warm bias. However, the quadrupole response is weaker in the nudged setup (not shown).

The remainder of this section discusses the $\overline{T}$ and $\overline{u}$ responses in the nudged setup 2 only.

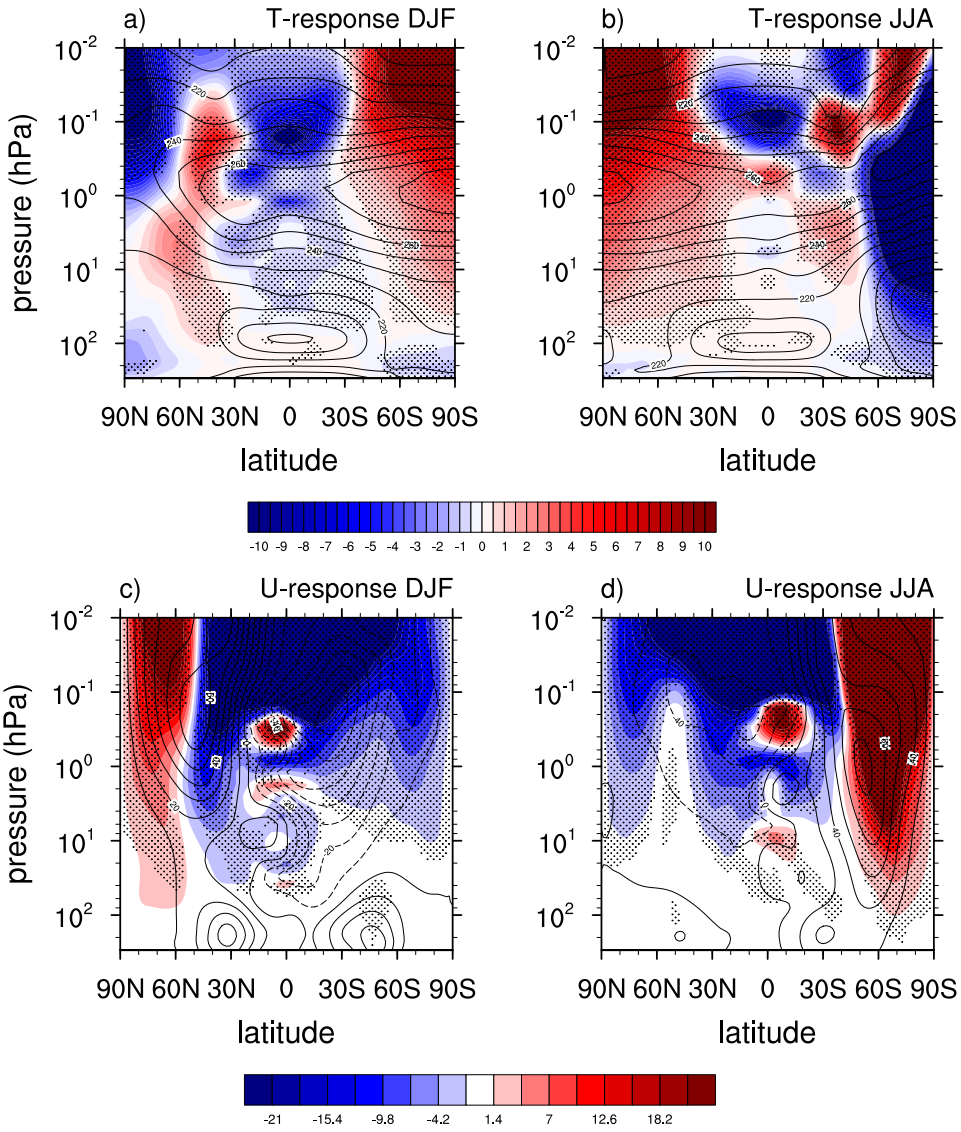

Figure 9: Same as Fig. 7 but for the nudged setup 2.

4.2.4 Orographic gravity wave drag

Figure 12 shows the $\overline{T}$ and $\overline{u}$ responses to the removal of OGWD in the nudged model. Since OGWD is largest in the NH winter (see Fig. 2), the larger response can be seen there. Interestingly, the removal of OGWD does not lead to cooling of the NH winter pole as would be expected from the linear response (i.e., less gravity wave drag, less downwelling and therefore less dynamical heating). Hence, either the resolved wave drag or the NOGWD responds by over-compensating for the absence of OGWD. The SH winter stratosphere experiences a small cooling in response to the absence of OGWD, consistent with the linear response.

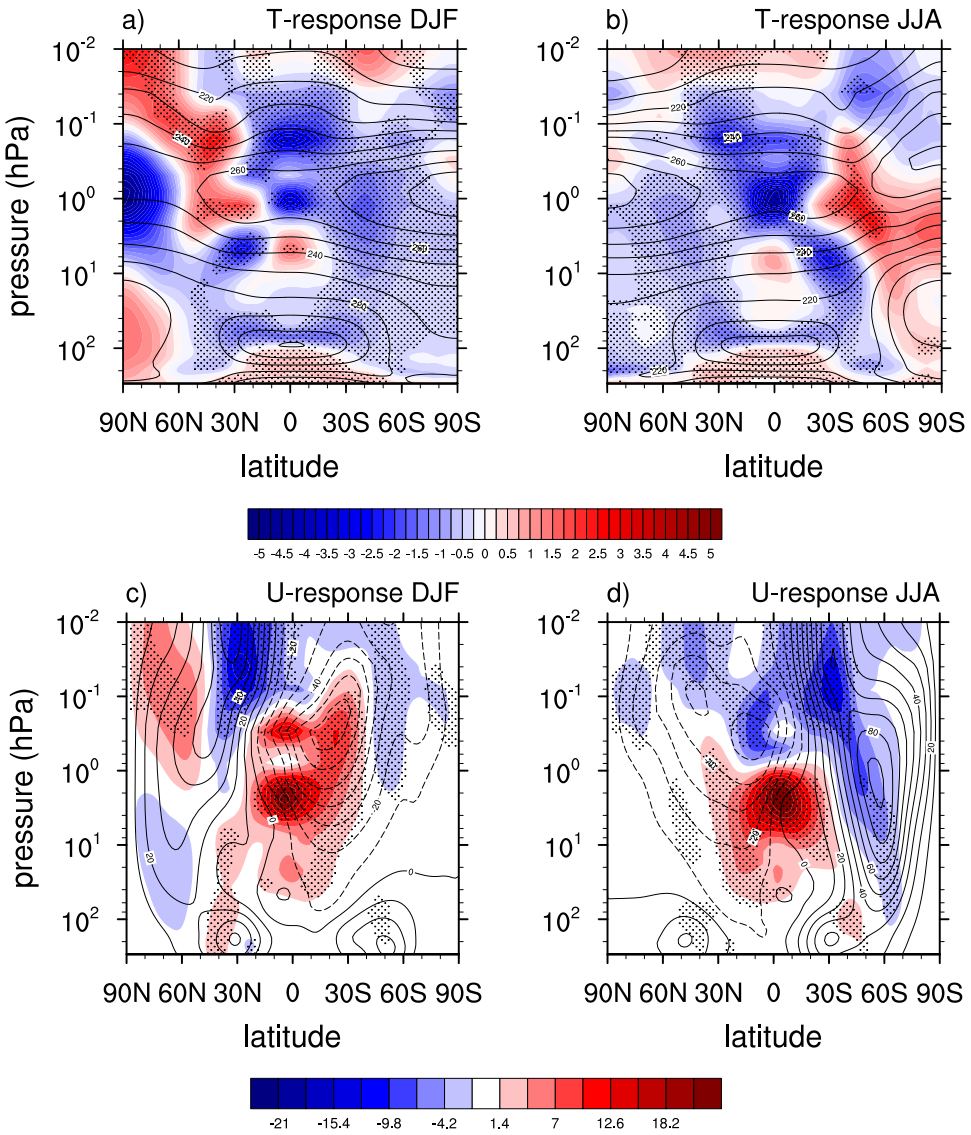

Figure 10: Same as Fig. 7 but for the response to the use of the TCo grid coupled to the SPPT parametrization. Notice the smaller contour interval compared to Fig. 7.

4.2.5 Radiation changes

The impact of the diurnal cycle in ozone, the reduction in solar UV output, and the absence of a sponge on $\overline{T}$ and $\overline{u}$ in the nudged model can be seen in Fig. 13. As already discussed in ECMWF (2017), the persistent global-mean warm bias in the mesosphere is drastically improved as a result of the radiative changes and the removal of the sponge. Additionally, the upper- to mid-stratospheric SH winter warm bias is also somewhat improved by the radiation and sponge changes.

4.3 Section summary

- Persistent temperature biases against MLS and ERA-I include: a ∼10 K warm bias in the winter SH stratosphere centered at 55 °S, a global warm bias of 20 K in the mesosphere and upper strato-

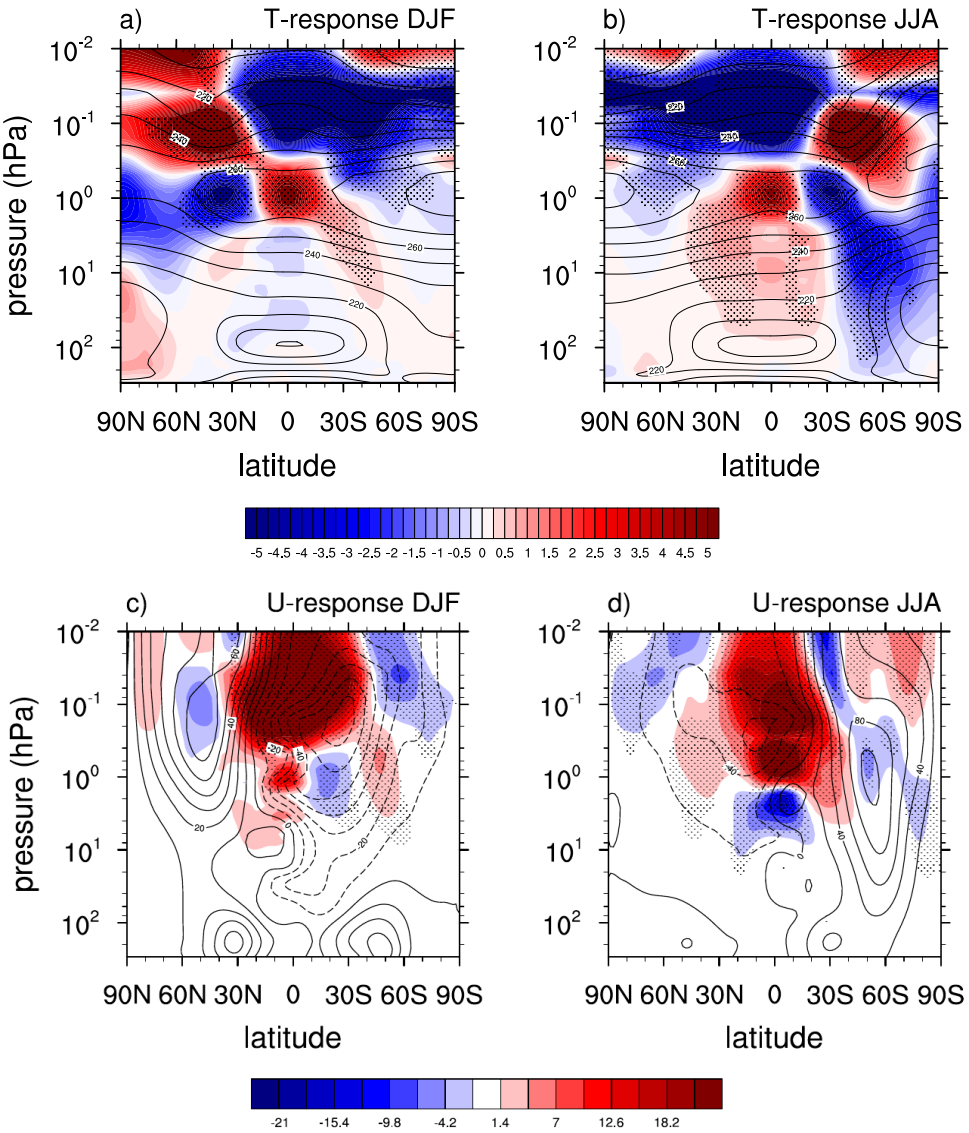

Figure 11: Same as Fig. 7 but for response to no sponge.

sphere, a 5 K cold tropopause bias over high latitudes (largest in NH summer), and a 3 K cold bias over the tropical lower stratosphere when evaluated against ERA-I only.

- Introduction of the diurnal cycle of ozone and the reduction in solar UV output in the radiation scheme together with the removal of the sponge eliminate the global-mean mesospheric and upper-stratospheric warm bias.
- NOGWD has a strong influence on the circulation in the summer hemisphere, with stronger NOGWD resulting in cooling that is consistent with stronger upwelling. NOGWD also strongly affects the winter hemisphere polar temperatures, with stronger NOGWD resulting in more warming, especially over the SH winter pole. OGWD has a much smaller impact on the temperature structure.
- Use of a higher-resolution TCo grid coupled to the SPPT scheme cools the tropical lower stratosphere and the summer hemisphere stratosphere by $\sim$2 K, exacerbating the tropical cold bias at

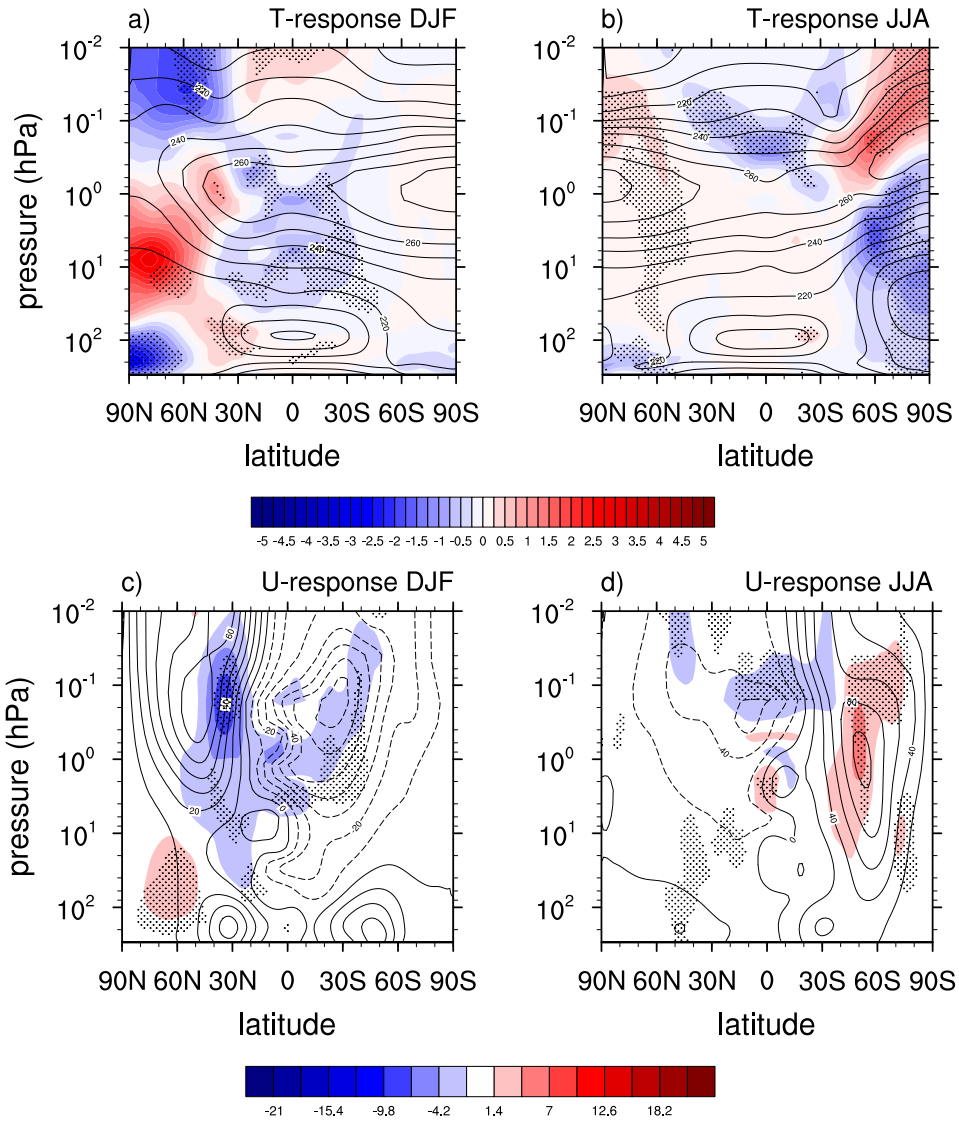

Figure 12: $\overline{T}$ and $\overline{u}$ responses for (a) DJF and (b) JJA to switching off OGWD in the nudged setup 2.

the tropopause. Much of the same behaviour is also seen with horizontal resolution increase in general, irrespective of the type of grid used (i.e., TCo or TL).

- The current sponge formulation warms the mesosphere by ∼5 K and produces a quadrupole response in the winter hemisphere. There is a hint that the removal of the sponge alleviates the SH winter stratospheric warm bias.

- None of the model changes that affect the momentum budget completely eradicate the warm mid- to high-latitude upper-stratospheric SH winter bias. This hints to this bias having a radiative origin.

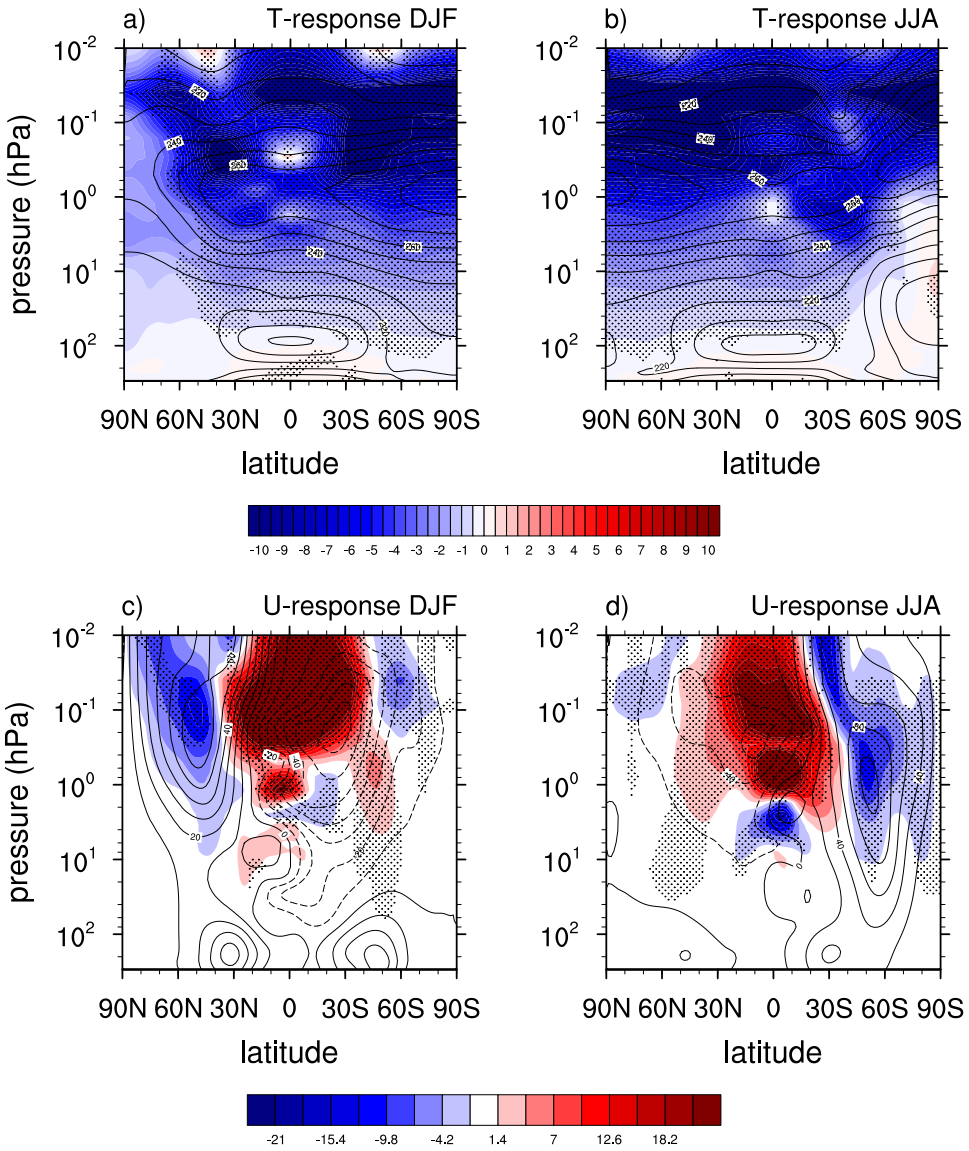

Figure 13: Same as Fig. 12 but for the response to reduced UV, inclusion of an approximate diurnal cycle of ozone and the removal of the sponge.

5 The Brewer-Dobson circulation

5.1 The tropical tape recorder signal

Water vapour enters the stratosphere through the tropics and spreads upward and poleward by the action of the BDC. Water vapour above the tropical tropopause layer behaves almost like a passive tracer, whose concentrations are determined by the annual cycle in the tropical tropopause temperatures. The tropical tape recorder signal in the lower stratosphere (Mote et al. 1996) is understood to be a result of water vapour advection upward by the BDC. Hence, the tape recorder signal has often been used as a proxy for the upwelling speed of the BDC. Recently, Glanville & Birner (2017) found that the vertical transport velocity inferred from the tropical tape recorder signal in ERA-I reanalysis and in NASA's Goddard Earth

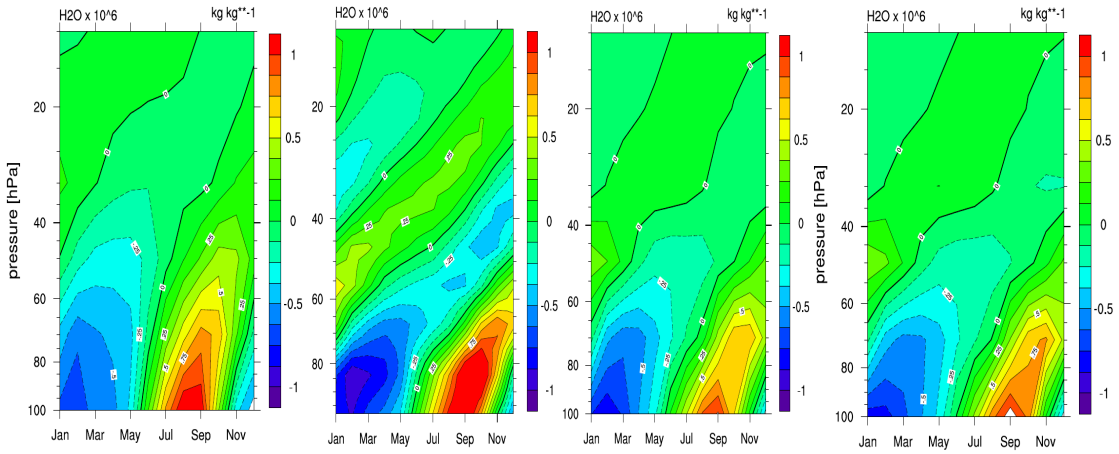

Figure 14: The tropical tape recorder signal in (a) ERA-I, (b) MLS, (c) the control run for setup 1, and (d) the run where the vertical diffusion is reduced in the upper troposphere and stratosphere. The figures show yearly composites from 2004 to 2014. To compute the tape recorder signal, the time and zonal-mean specific humidity field is first subtracted from the 6-hourly zonal-mean specific humidity field. This is then averaged in latitude between 15 °N and 15 °S.

Observing System Chemistry Climate Model is a factor of two to five (depending on the season) stronger at 80 hPa than the residual vertical velocity and a factor of four stronger than the tape recorder signal in HALOE and MLS observations (see their Fig. 2 and 4). They concluded that vertical diffusion plays a dominant role in driving the tropical tape recorder signal with a lesser contribution from the residual mean vertical velocity. The effect of diffusion on the tropical tape recorder signal has previously been discussed in (Mote et al. 1998).

Figure 14 shows the composites of the tropical tape recorder signal between 2004 and 2014 for the ERA-I, MLS and the control run from setup 1. As in Glanville & Birner (2017) it is also found that the ERA-I tape recorder signal is considerably faster than the MLS observations, especially above 80 hPa. This is also the case for the control integration. It takes air originating at 80 hPa ∼8 months to reach 40 hPa in MLS observations, whereas in ERA-I it takes ∼2 months and in the control run ∼5 months. This translates to tropical vertical velocities of 0.23 mm s^{-1} for MLS, 0.9 mm s^{-1} for ERA-I, and 0.37 mm s^{-1} for the control run (using the scale height value of 7 km). This makes the tape recorder signal about a factor of four too fast in ERA-I and about a factor of two too fast in the control run in comparison to MLS. The estimate for the control run is not too far off from the annual mean tropical residual vertical velocity speed. Thus, the tape recorder signal in the control run is less affected by diffusion than ERA-I. The weaker diffusion in CY43R1 can be due to different model numerics/physics in cycle CY43R1 compared to the much earlier cycle used in ERA-I: For example, higher horizontal and vertical resolutions generally reduce numerical diffusion. Note that water vapour is not assimilated in the stratosphere in ERA-I, and by comparing the tropical tape recorder signals in ERA-I and in the free-running model, we are mainly comparing the numerical models. Notably, the tape recorder signal in ERA-5 closely resembles the control run tape recorder (not shown).

To study the effect of the parameterized vertical diffusion on the tape recorder signal, experiments have been performed where parametrized vertical diffusion is switched off above 400 hPa in the tropics only. The tape recorder signal from this simulation is shown in Fig. 14d. The impact of the reduced parameterized vertical diffusion on the tropical tape recorder signal is, however, negligible (cf. Fig. 14c with Fig. 14d).

It should be noted that NOGWD flux changes have no impact on the tropical tape recorder signal (not shown) [4]. This is perhaps not surprising as NOGWD is weak in the tropical lower stratosphere (see Fig. 2) and its impact on the tropical upwelling is small (see ahead to the next section), unlike at higher latitudes where NOGWD contributes significantly to the downwelling. Increase in the physical space resolution brought about by the use of the TCo grid at T255 truncation also has no impact on the tropical tape recorder signal (not shown).

5.2 The residual mean meridional circulation

5.2.1 The control run: Time-mean circulation

Figure 15 shows the annual-mean tropical upward mass flux (a) and the extended winter mean (October-May for the NH and March-November for the SH) downward mass flux over the NH (b) and SH (c) polar caps for the control run. The extended winter period comprises all the months for which polar-cap downwelling occurs. Both the total downward control mass flux and the parametrized wave contribution are shown. The downward control and the direct streamfunctions disagree slightly over the extended SH winter pole due to the transience of the vortex breakdown process.

Table 3 summarizes the resolved and parametrized wave partitioning in driving the tropical upwelling and extended winter polar cap downwelling in both hemispheres. At 70 hPa, parameterized waves account for 7% of the total upwelling (5% OGWD and 2% NOGWD) decreasing to 0% (2.4% OGWD and -2.4% NOGWD) at 10 hPa. These figures should be compared to the multi-model inter-comparison of Butchart et al. (2011), where on average parameterized waves account for 28% of the upwelling (21.1% OGWD and 7.1% NOGWD) at 70 hPa and 25.6% (4.7% OGWD and 10.9% NOGWD) at 10 hPa. Given the higher horizontal resolution of the IFS compared to the models in Butchart et al. (2011) it is not surprising that the role of parameterized wave drag is smaller in the IFS than in these studies. Note that the relative role of parametrized waves in driving the upwelling increases as one approaches tropopause in Fig. 15a. This is a result of the NOGWs being launched at 450 hPa and the westward propagating NOGWs breaking at the critical levels in the subtropics, where the subtropical jets terminate. Hence, the location of the NOGW launch level is likely to impact the parametrized waves that contribute to the tropical upwelling.

There are large differences in the parameterized wave downwelling magnitudes between the hemispheres. At 70 hPa, parameterized waves account for only 7% (all OGWD) of the total extended NH winter pole downwelling, while in the SH the similar figure is 19%. In the SH all of the parameterized downwelling is coming from NOGWD. This is expected from Fig. 2, which shows much larger influence of NOGWD in the SH than in the NH. Generally, the ratio of the parameterized to resolved wave drag in driving the upwelling decreases slightly with altitude in the tropics, and increases with altitude over the poles (see Table 3). The parameterized wave downwelling starts to dominate the resolved wave downwelling above 5 hPa in the SH and above 1 hPa in the NH.

5.2.2 The control run: The seasonal cycle

To understand how the partitioning of parameterized and resolved waves in driving the polar cap downwelling differs between seasons and between the hemispheres, it is useful to examine the seasonal cycle of the polar cap average $\overline{w}^*_{DC}$ as in Shaw et al. (2009). Figure 16 shows the seasonal cycle of polar cap

[4] The tropical tape recorder signal can only be constructed from runs that are over one year in duration.

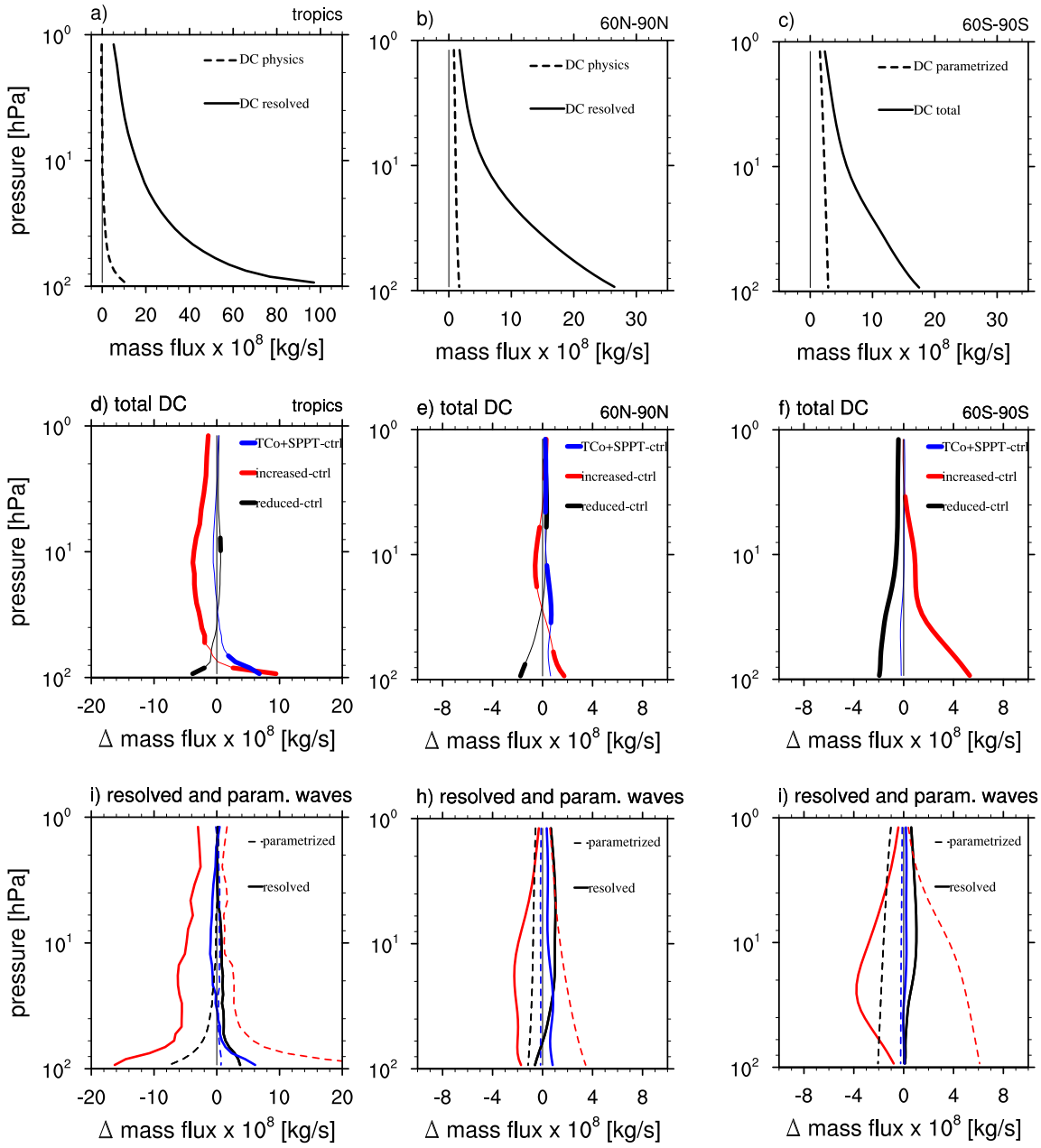

Figure 15: (a) Annual-mean tropical upward mass flux and extended winter downward mass flux over (b) the NH and (c) the SH polar cap (poleward of 60 °N/S) for the control run. The total downward control streamfunction is shown in solid lines and the parametrized wave contribution is shown in dashed lines. (d-f) Response in total downward control mass flux over (d) the tropics, (e) the NH pole and (f) the SH pole to a decrease in NOGWD (in black), increase in NOGWD (in red), and to the use of the TCo grid coupled to SPPT (in blue). The thickened lines in the response plots show regions where the response is significant at the 95% level by the Student-t test on the means. (g-i) Same as (d-f) but the response is separated into the resolved wave contribution (solid lines) and the parametrized wave contribution (dashed lines) to the downward control streamfunction.

Table 3: Resolved and parametrized (OGWD and NOGWD) wave contribution (in % of the total) to the annual-mean tropical mass flux and extended winter (Mar-Nov for the SH, and Oct-May for the NH) polar cap downward mass flux for the control, reduced NOGWD and increased NOGWD runs at 10 hPa and at 70 hPa. Positive percentage denotes tropical upwelling and polar cap downwelling and negative percentage denotes tropical downwelling and polar cap upwelling.

Experiment	Region	Pressure [hPa]	Parametrized wave drag [%]			Resolved wave drag [%]	Mass flux $\times 10^8$[kg/s]
			OGWD	NOGWD	All		
Control	Annual-mean upwelling	10	2.4	-2.4	0	100	15.5
		70	5	2	7	93	58.1
	NH polar cap downwelling	10	14	5	19	81	5.7
		70	7	0	7	93	22.2
	SH polar cap downwelling	10	0	40.6	40.6	59	5.8
		70	0	19	19	81	15
Reduced NOGWD	Annual-mean upwelling	10	2.5	-3	-0.5	100.5	16.1
		70	5	-3	2	98	57.1
	NH polar cap downwelling	10	14	-9	5	95	6.2
		70	8	-6	2	98	20.7
	SH polar cap downwelling	10	0	12	12	88	5.4
		70	0	6	6	94	13.5
Increased NOGWD	Annual-mean upwelling	10	4	6	10	90	11.8
		70	4	16	20	80	57.4
	NH polar cap downwelling	10	7.5	38.5	46	54	5.2
		70	5	14	19	81	23.2
	SH polar cap downwelling	10	0	88	88	12	6.7
		70	0	45	45	55	19.3

average $\overline{w}^*_{DC}$ (thick solid lines) and its parameterized wave (dashed lines) and resolved wave (thin solid lines) contribution for the control simulation (black lines).

Consistent with the diagnostics in Fig. 2, the upwelling in the summer mesosphere is solely driven by NOGWD over both poles with no contribution from the resolved gravity waves. In the NH, the downwelling is maximum in mid-winter in January and is predominantly driven by resolved waves in the stratosphere (apart from the upper-stratosphere where the parameterized waves dominate the downwelling in autumn). In the NH the parametrized wave downwelling is maximum during the stratospheric zonal wind maximum in the late autumn/early winter, whereas the maximum in the resolved wave downwelling is offset slightly in time. In contrast, in the SH the downwelling is maximal in the spring season and the time of maximum downwelling occurs later as one descends through the stratosphere. The resolved waves dominate the downwelling in the spring season, whereas the parameterized waves dominate the downwelling in mid-winter in the mid- to upper-stratosphere (see also Fig. 2), at the time of maximum westerlies. This seasonal behaviour of the resolved and parametrized waves is consistent with observations (e.g., Randel 1988, Quintanar & Mechoso 1995, Pulido & Thuburn 2008) and also observed in the Canadian Middle Atmosphere Model (CMAM) (Shaw et al. 2009). The different timing in the resolved and parameterized wave downwelling will be important for the response in the seasonality of $\overline{w}^*_{DC}$ to changes in NOGWD. Note that unlike in the lower-resolution models, OGWD does not contribute to the polar cap averaged $\overline{w}^*_{DC}$ in the SH (not shown).

5.3 Impact of model changes on the residual mean meridional circulation

5.3.1 Non-orographic gravity wave drag: Time-mean circulation

Given the importance of NOGWD at higher resolution, the sensitivity of tropical upwelling and polar cap downwelling to changes in NOGWD flux is now examined. Table 3 summarizes the changes to resolved and parametrized wave partitioning brought about by a decrease in NOGWD flux by 3.75 times and an increase in NOGWD flux by 3.75 times. As expected, the parametrized wave driving decreases (increases) with a decrease (increase) in NOGWD flux. For example, at 70 hPa parametrized wave contribution to the tropical upwelling and NH polar cap downwelling reduces to 2% with a reduction in NOGWD flux. Similarly, parametrized wave contribution to the 70 hPa tropical upwelling and NH polar cap downwelling increases to nearly 20% with an increase in NOGWD flux. For the SH polar cap downwelling, the similar figure is 6% for a decrease in NOGWD flux and 45% for an increase in NOGWD flux.

Figure 15 shows the response in the annual-mean tropical upward mass flux (d and g) and the extended NH (e and h) and SH (f and i) winter downward mass flux to decrease in NOGWD flux by 3.75 times (black lines) and increase in NOGWD flux by 3.75 times (red lines). As expected from the dominance of NOGWD in the SH, varying NOGWD flux has the most impact there. In particular, the total downwelling increases in response to increase in NOGWD (see Table 3). For example, increasing NOGWD flux from the control value by 3.75 times leads to a $\sim$30% increase in the SH polar cap downwelling at 70 hPa. The net effect of the increased downwelling is to warm the SH stratospheric winter pole (Fig. 8). However, the response in the total downwelling is not directly proportional to the change in NOGWD induced downwelling (dashed lines in Fig. 15g-i) as the resolved wave downwelling (solid lines in Fig. 15g-i) opposes the NOGWD changes in the time-mean. Interestingly, in the NH polar mid- and upper-stratosphere and in the tropics, the decrease in the resolved wave driving in response to increase in NOGWD leads to a decrease in total downwelling (see Table 3).

To understand the changes in the resolved wave forcing, Figs 17a-b show the difference in the extended

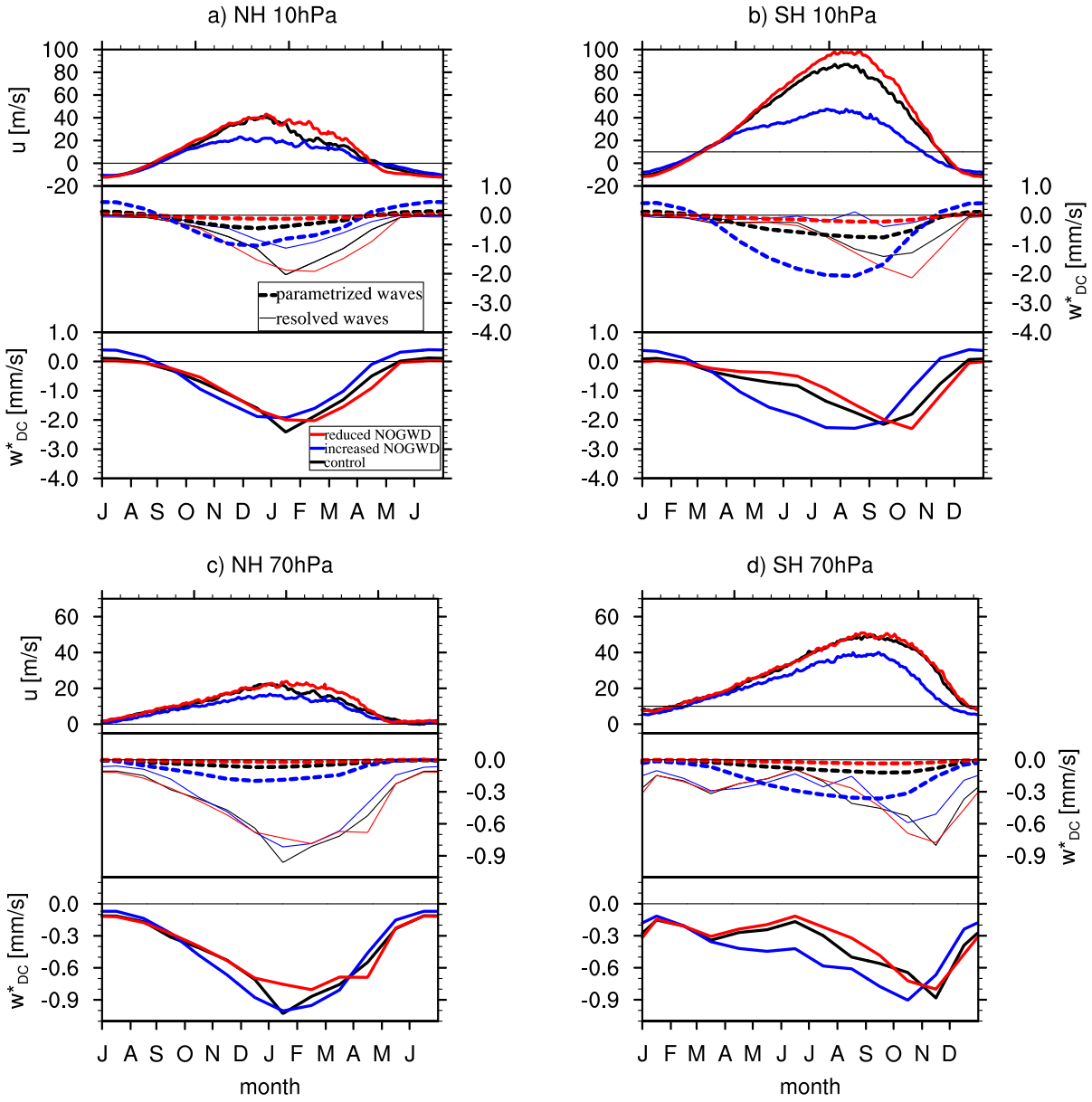

Figure 16: Seasonal cycle of $\overline{w}^*_{DC}$ (thick lines, bottom panels in each figure), split into its parameterized wave (dashed lines, middle panels in each figure) and resolved wave (thin solid lines, middle panels in each figure) contributions averaged over the (a,c) NH and (b,d) SH polar cap (between 60-85 °N/S) at (a,b) 10 hPa and (c,d) 70 hPa, respectively. Black lines denote the control run, red lines reduced NOGWD run, and blue lines increased NOGWD run, respectively. Note that the time-axis has been shifted by six months in (a,c) for clarity. The seasonal cycle in the zonal-mean zonal wind at 60 °N/S is shown for reference in the top panels.

NH and SH winter stratospheric EP flux and its divergence between the increased and reduced NOGWD runs. The resolved wave drag corresponds to EP flux convergence, hence the red regions indicate less wave drag. Over the polar vortex, the resolved wave response falls into two distinct regions: an increase in the resolved wave breaking in the lower-stratosphere and a decrease in the resolved wave breaking in the mid- to upper-stratosphere. This is reflected in the resolved wave response in Fig. 15h and 15i (solid lines) that sees a downward shift in the resolved wave downwelling.

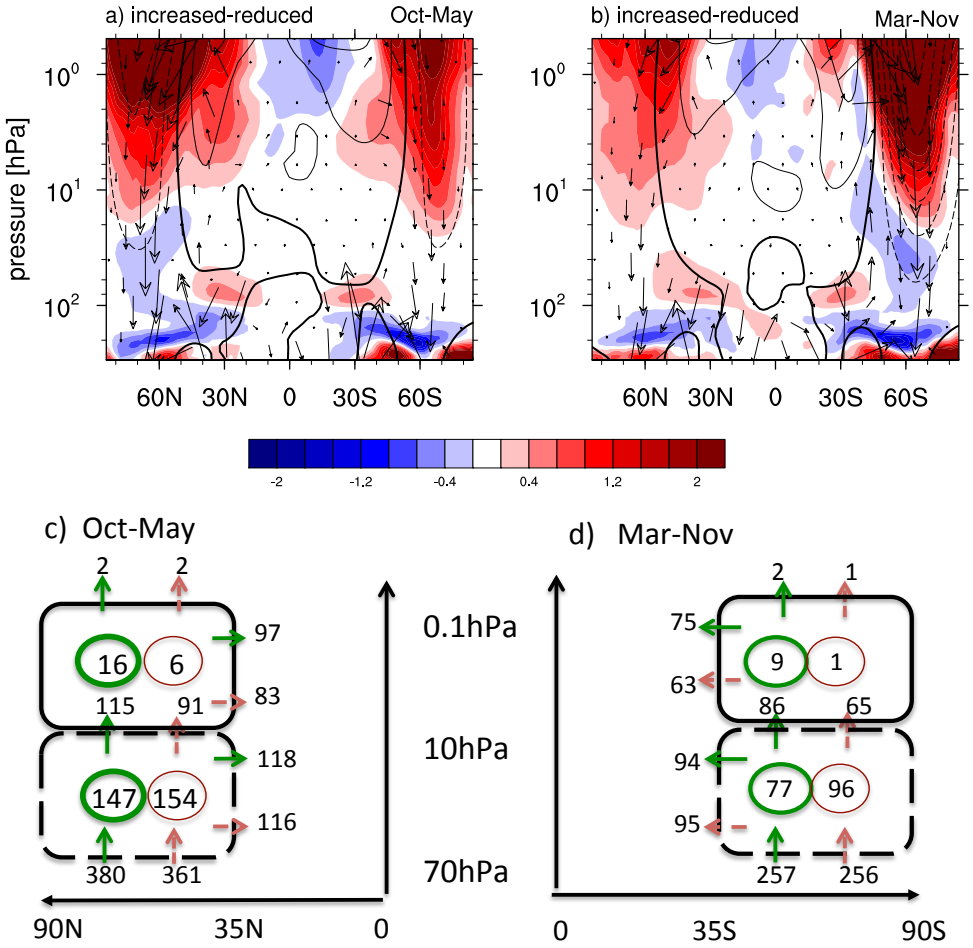

Figure 17: (a-b) Latitude-pressure cross sections of the resolved wave drag difference (in shading, units m s^{-1} day^{-1}) between the increased and reduced NOGWD runs for the extended (a) NH (Oct-May) and (b) SH (March-November) winters. The EP flux vectors are shown by the arrows. The zonal-mean zonal wind difference (m s^{-1}) is shown in black contours (contour interval 10 m s^{-1}), negative contours are dashed and the zero contour is drawn with double thickness. (c-d) The EP flux budget (in $\times 10^{16}$ N m) for the extended (c) NH and (d) SH winters for the reduced NOGWD (in green) and increased NOGWD run (in red) for the two boxes (see text). The positive numbers inside the boxes show the net resolved wave convergence (i.e., the wave breaking). The vertical arrows represent heat fluxes and the horizontal arrows represent momentum fluxes.

To quantify the response in the resolved waves in the lower- and upper-stratosphere, an EP-flux budget (following Kushner & Polvani (2004)) is constructed for two boxes in the vicinity of the polar vortex between 35 °N/S and 90 °N/S: 1) a lower-stratospheric box from 70 to 10 hPa and 2) an upper-stratospheric/lower-mesospheric box from 10 to 0.1 hPa. The budget is shown for the increased (in red) and reduced (in green) NOGWD runs in Fig. 17c-d. In the winter lower-stratosphere (10-70 hPa boxes) there is 5% more wave drag in the NH and 25% more wave drag in the SH in the increased NOGWD run compared to the reduced NOGWD run (i.e., $100 \times (154-147)/147$ for the NH, and $100 \times (96-77)/77$ for the SH). This likely occurs as a result of weakened vortex —brought about by the increase in NOGWD– that is more amenable to wave breaking lower down. There is a marked reduction in the resolved waves entering (21% less in the NH and 25% less in the SH — i.e., $100 \times (91-115)/115$ for the NH, and $100 \times (65-86)/86$ for the SH) and breaking (63% less wave breaking in the NH and 89% less wave breaking in the SH — i.e., $100 \times (16-6)/6$ for the NH, and $100 \times (1-9)/9$ for the

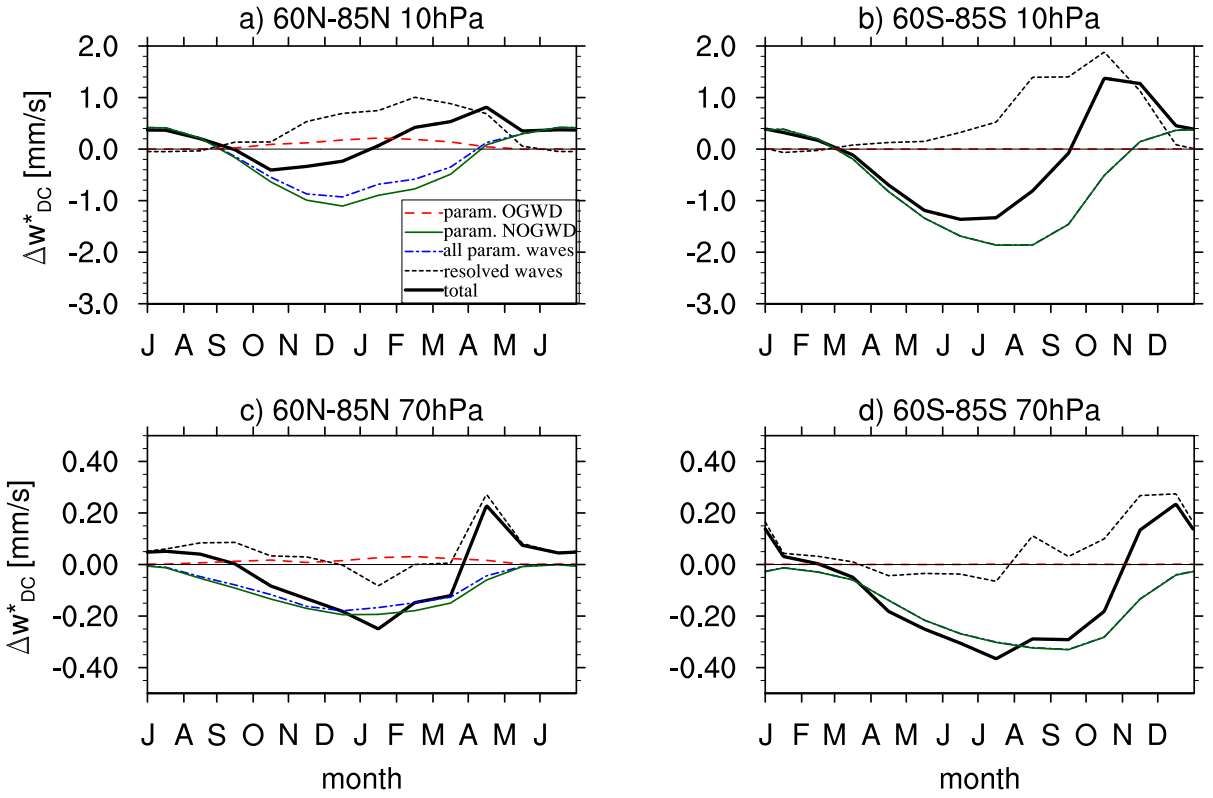

Figure 18: Seasonal cycle of the difference in $\overline{w}^*_{DC}$ (thick black lines) between the increased and reduced NOGWD runs, split into its parameterized wave (dash-dotted blue lines) and resolved wave (dotted black lines) contributions. The NOGWD change is shown in solid green and the OGWD change is shown in dashed red. $\overline{w}^*_{DC}$ response averaged over the (a,c) NH and (b,d) SH polar cap at (a,b) 10 hPa and at (c,d) 70 hPa.

SH) in the upper-stratosphere (10-0.1hPa boxes) in the increased NOGWD run compared to the reduced NOGWD run.

Figures 20-22 show the winter/spring mean tropical and polar-cap mass flux responses to a decrease (black lines) and an increase (red lines) in NOGWD in the nudged setup. Qualitatively, the response to NOGWD perturbations in the nudged runs is similar to that in the free-running setup.

In summary, increasing NOGWD weakens the polar night jet and thereby decreases resolved wave propagation into the polar mid- to upper-stratosphere during the extended winter season, leading to less resolved wave breaking there. This counteracts the polar cap downwelling increase by the NOGWD such that the total mid- to upper-stratospheric downwelling decreases in the NH and increases in the SH in response to increase in NOGWD. In the lower-stratosphere the polar cap downwelling increases in both hemispheres as the resolved waves reinforce the NOGWD perturbation. The nudged setup for one NH and SH extended winter qualitatively reproduces the response in polar cap downwelling observed in the long free-running runs. The nudged runs give statistically significant results with only five ensemble members. This makes the nudging framework attractive to use for understanding the BDC sensitivity to model changes that directly affect the middle-atmosphere circulation.

5.3.2 *Non-orographic gravity wave drag: The seasonal cycle*

The time-mean response might paint a misleading picture of the interaction between the resolved and the parameterized waves as there is a strong seasonality in the BDC forcing. The seasonal cycle of the polar cap average $\overline{w}^*_{DC}$, together with its resolved and parameterized wave driving contributions, is also shown in Fig. 16 for the reduced NOGWD run (in red) and increased NOGWD (in blue) for the free-running setup. Figure 18 shows the seasonal cycle of the difference in the polar cap average $\overline{w}^*_{DC}$ between the increased NOGWD and reduced NOGWD runs.

In the summer, the total $\overline{w}^*_{DC}$ response in the upper-stratosphere is proportional to changes in NOGWD as the easterlies filter stationary planetary waves and smaller scale orographic gravity waves, leaving no resolved waves to interact with (see Fig. 2). Note that the change from downwelling to upwelling occurs earlier in the increased NOGWD run, especially in the SH. This appears to be tied in with the onset of the final warming that occurs earlier in the increased NOGWD run (see Fig. 16b); because the westerlies weaken earlier in the increased NOGWD run, the eastward propagating NOGWs can get through into the upper-stratosphere and mesosphere earlier. When the eastward propagating waves saturate they induce upwelling.

To further examine the effect of NOGWD on the final warming date, Fig. 19 shows the average of the final warming dates in the SH as a function of pressure together with the ERA-Interim climatology from 2004 to 2015 for reference (thick black dash-dotted line). As the NOGWD is increased, the climatological final warming date occurs earlier in the stratosphere as the vortex is weakened and is thus more amenable to wave breaking. This is consistent with more resolved wave drag in the lower-stratosphere (see Fig. 17b). In the mesosphere, however, the vortex breakdown is delayed when the NOGWD is substantially increased. This is, as discussed above, due to the reduced resolved wave drag entering the upper-stratosphere and mesosphere. Resolved wave drag accelerates the seasonal evolution towards easterlies in the spring, so when it is reduced, the seasonal cycle is delayed. Note that the NOGWD tends to drag the zonal winds to zero at mid- to high-latitudes near the model top as the waves, originating at 450 hPa, are filtered such that only those with phase speeds of opposite sign to the zonal wind are left. Therefore NOGWD does not contribute to the vortex breaking in the same way as the resolved waves. It should be emphasized that here the NOGWD is reduced via the sources, but the total resolved wave drag is unchanged, only its location is altered.

In the NH, OGWD partly compensates for the increase in NOGWD induced downwelling during winter (cf. dashed red, solid green and dash-dotted blue curves in Figs. 18a and 18c). The resolved wave drag shifts vertically in response to increase in the NOGWD induced downwelling in the mid- to upper-stratosphere (cf. dotted lines in Figs 18a and 18c), but there is a seasonal offset in the resolved wave response.

The seasonal offset in the resolved wave response is larger in the SH, where the changes to NOGWD flux significantly modify the seasonal evolution of polar cap averaged $\overline{w}^*_{DC}$. When NOGWD is increased, it has the most impact in mid-winter in the SH when the resolved wave driving is weak in the stratosphere. Hence, the change in the SH total polar cap averaged $\overline{w}^*_{DC}$ is almost proportional to NOGWD flux changes in mid-winter. Increasing NOGWD weakens and shifts the polar night jet equatorward. This leads to less resolved waves entering the mid- to upper-stratosphere—especially in the SH spring—resulting in less resolved wave downwelling (see Fig. 18). The resolved waves appear to be unable to propagate as high into the stratosphere in the increased NOGWD run. As the parameterized wave downwelling is weak in the spring, the decrease in the resolved wave downwelling dominates and results in a decrease in downwelling with increase in NOGWD. In the lower-stratosphere (Figs. 18c-d), the resolved waves tend to amplify the NOGWD changes in mid-winter in both hemispheres, consistent with the increased

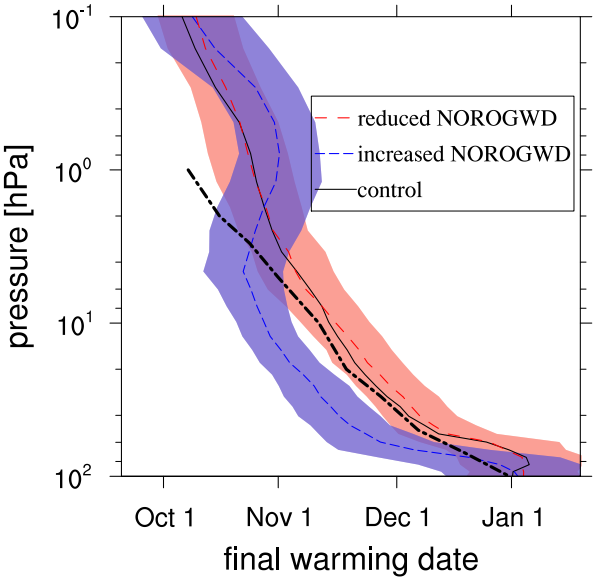

Figure 19: Average of the final warming dates in the SH for the control run (solid black), the reduced NOGWD run (long-dashed red) and the increased NOGWD run (short-dashed blue). The average of the ERA-Interim final warming dates between 2004 and 2015 is shown in thick dot-dashed black contour. The shading shows the 2-σ interval for the increased and reduced NOGWD runs only. The Black & McDaniel (2007) method is used to diagnose the final warming date in the SH. In particular, a final warming occurs when the zonal-mean zonal wind at 60 °S falls below 10 m s^{-1} and does not return to values above 10 m s^{-1} before the next winter.

wave breaking in the mid-latitude lower-stratosphere shown in Figs. 16 and 17.

5.3.3 TCo grid and SPPT

The blue lines in Fig. 15d-i show the response in the tropical upward and polar downward mass fluxes to the use of the higher-resolution TCo grid and SPPT in the free-running model. Both these options are enabled in the seasonal forecasting system at ECMWF. Because the interest is placed here on seasonal timescales, it makes sense to investigate the BDC sensitivity to both these options together. It is clear from the figure that TCo+SPPT has a much smaller influence on the polar cap downwelling than the NOGWD changes. The tropical upwelling in the lowermost stratosphere increases, however, with the use of TCo+SPPT, resulting in 1-2 K cooling there. The increase in the upwelling is occurring via an increase in the resolved wave drag. The weak mass flux response is consistent with the weak temperature response in Fig. 10.

The dark blue lines in Figs. 20-22 show the effect of TCo+SPPT on the polar cap downwelling and tropical upwelling in the nudged setup. The TCo+SPPT has a bigger impact on the BDC than in the free-running setup. The downwelling increases over the SH pole everywhere and over the NH pole in the mid- to upper-stratosphere. This is reflected by warming of the polar regions, especially in the SH. As in the free-running runs, the tropical upwelling in the lowermost stratosphere increases for both SH and NH extended winter conditions. Consistent with the increase in upwelling is a slight cooling of the tropical stratosphere. Therefore the use of TCo grid and SPPT is expected to result in cooling in the lower tropical stratosphere in all seasons.

The remainder of this section discusses the response in the tropical upwelling and the polar cap downwelling in the nudged framework only.

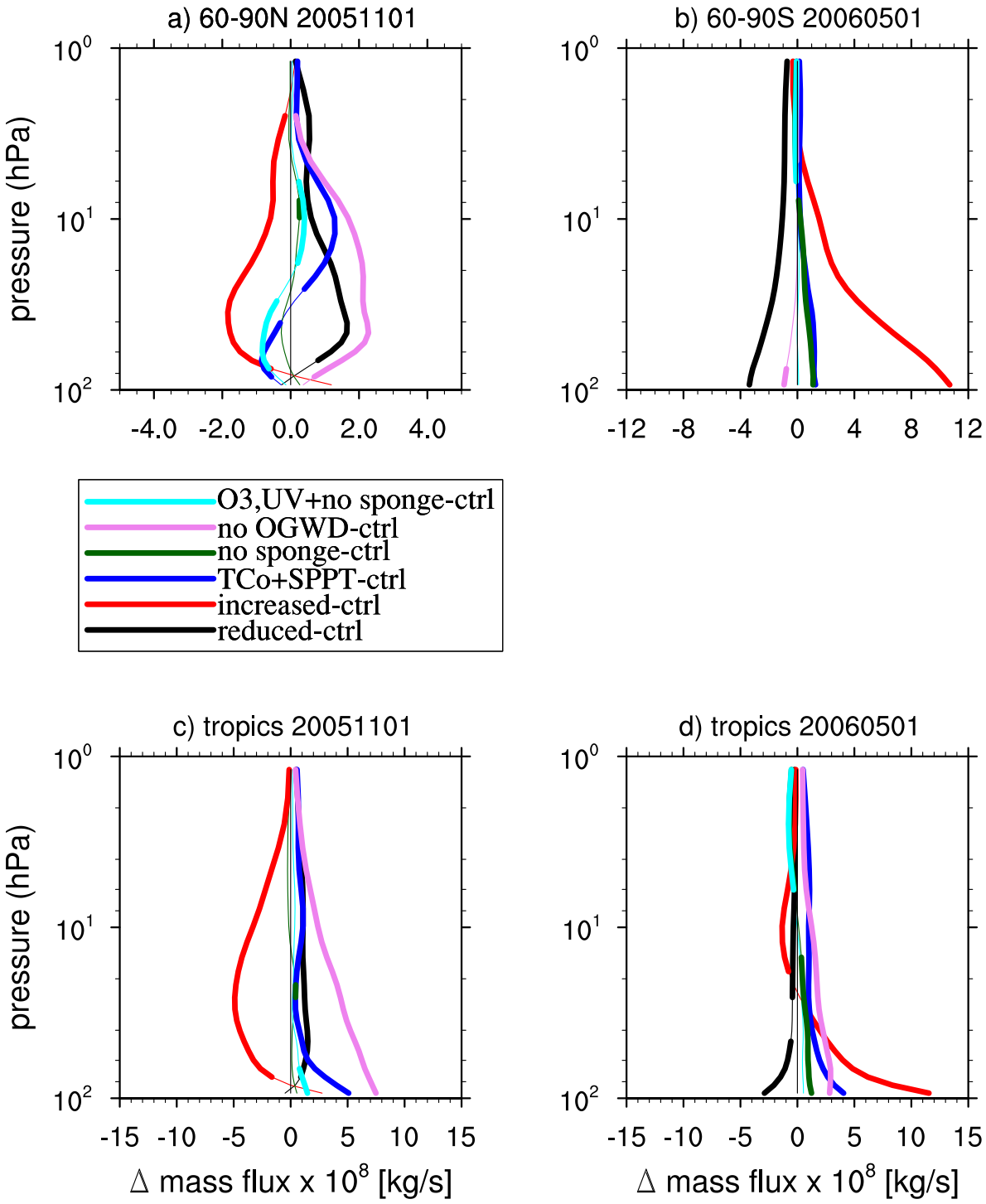

Figure 20: Response of the six month-mean (winter and spring seasons) mass flux to decrease in NOGWD flux (black lines), increase in NOGWD flux (red lines), the use of TCo grid with SPPT (blue lines), the absence of sponge (green lines), the absence of OGWD (pink lines), and the diurnal cycle of ozone, reduction in solar UV output and the absence of sponge (cyan lines) for the nudged setup. (a,b) Polar cap downwelling. (c,d) Tropical upwelling. (a,c) Downwelling and upwelling for the forecast started on (a,c) 01/11/2005 and on (b,d) 01/05/2006, respectively. The thickened lines show regions where the response is significant at the 95% level by the Student-t test on the means.

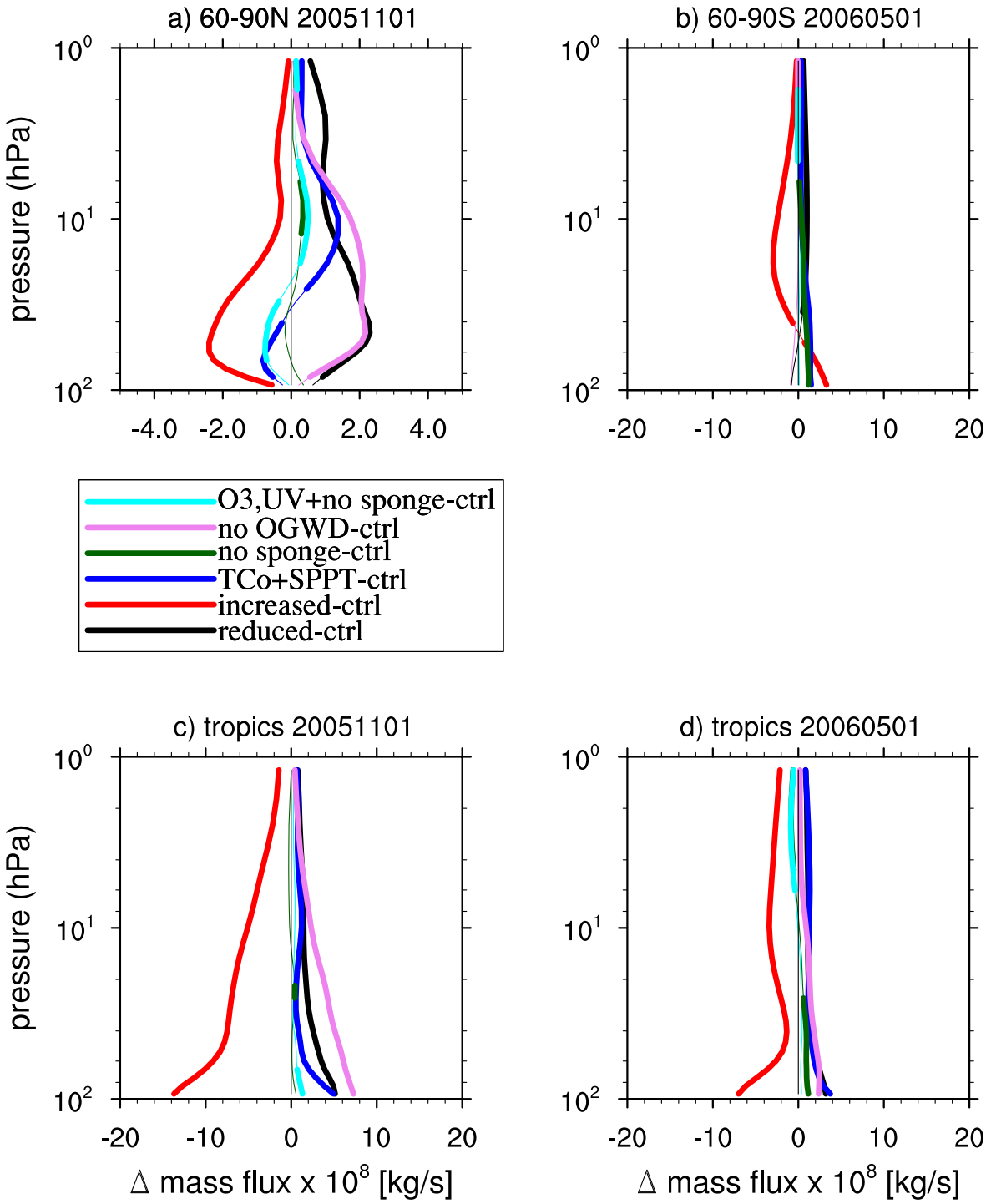

Figure 21: Same as Fig. 20, but for the response in resolved wave mass flux.

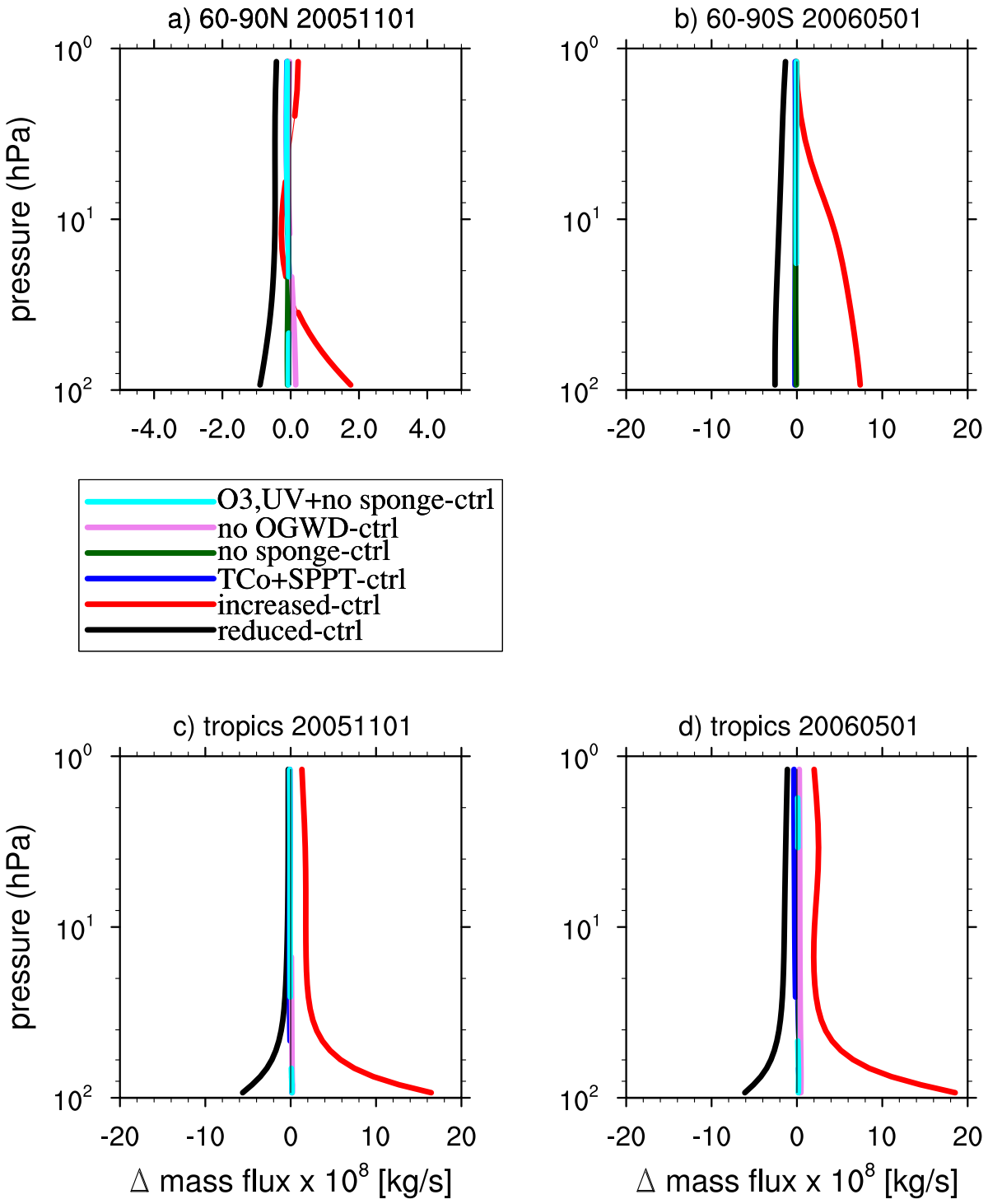

Figure 22: Same as Fig. 20, but for the response in parametrized wave mass flux.

5.3.4 *The sponge*

The effect of removing the sponge on the polar cap downwelling and tropical upwelling in the nudged setup is shown in the green lines in Figs. 20-22. The sponge has no impact on the BDC in the NH. In the SH, there is a slight increase in the polar cap downwelling in the absence of the sponge. This increase in SH polar cap downwelling occurs mostly in the spring season (not shown) and therefore does not show up as warming in the JJA mean temperature response in Fig. 13).

5.3.5 *Orographic gravity wave drag*

The impact of switching off OGWD on the BDC is shown for the nudged setup in the pink lines in Figs. 20-22. As expected from the dominance of OGWD in the NH, the largest response is seen there, with no change to downwelling over the SH winter pole. However, removing OGWD increases the downwelling in the NH and upwelling in the tropics. This occurs through the resolved wave drag. As the OGWD is removed, the zonal winds accelerate. This leads to an increase in NOGWD that compensates for the missing OGWD in the mid- to high-latitudes. Despite the complete compensation by the NOGWD, the zonal-mean zonal winds are altered by the increased NOGWD. This acts to increase the resolved wave forcing.

5.3.6 *Radiation changes*

The impact of the inclusion of an approximate diurnal cycle of ozone, the reduction in solar UV absorption and the absence of a sponge on the tropical upwelling and the polar cap downwelling can be seen in the cyan lines in Figs. 20-22. Compared to the response to removing the sponge (green lines in the Figs.), the SH polar cap downwelling does not change in this run. It is possible that the radiation changes affect the resolved-wave breaking such as to counteract the resolved-wave drag increase brought about by the removal of the sponge alone.

5.4 Section summary

- The tropical tape recorder signal is a factor of two too fast in the free-running model and a factor of four too fast in ERA-I compared to MLS observations. The signal is influenced by implicit (through semi-Lagrangian numerics) numerical model diffusion and therefore is not always a good measure of the residual mean meridional circulation.
- The tropical upwelling is mostly influenced by resolved-wave breaking in the lower stratosphere.
- The residual-mean meridional circulation is strongly influenced by NOGWD, especially in the SH. NOGWD accounts for all the upwelling over the summer hemisphere polar cap. The maximum in the parameterized and resolved wave downwelling over the polar cap is offset in time; the parameterized waves dominate earlier in the winter and the resolved waves dominate later in the winter/early spring. This offset is larger in the SH. OGWD plays no role in polar cap downwelling over the SH.
- The change to the NOGWD flux has the largest influence on the BDC both in the free-running and in the nudged model. The resolved wave response counteracts the NOGWD perturbation in the polar mid- to upper-stratosphere and amplifies the perturbation in the polar lower stratosphere.

Due to the different partition of the resolved and parameterized waves in driving the downwelling between the two hemispheres, the response in the total polar cap downwelling is different between the NH and the SH: The total downwelling increases with increase in NOGWD flux in the SH, whereas it decreases in the NH. OGWD counteracts the NOGWD changes in the NH.

- The resolved and parameterized wave interaction does not occur instantaneously: During early winter, when the parameterized waves dominate the polar cap downwelling, the response is proportional to changes in NOGWD. In the late winter/spring, however, the downwelling response is dominated by the resolved wave response.
- The use of TCo grid coupled to the SPPT scheme, the absence of a sponge, and radiative changes have a lesser impact on the polar cap downwelling. There is a robust response to TCo+SPPT in the tropics, where the upwelling increases due to an increase in the resolved wave driving in the lower stratosphere.
- The absence of OGWD in the nudged framework has an impact on the polar cap downwelling in the NH and on the tropical upwelling. Counter-intuitively, excluding OGWD leads to an increase in the strength of the polar cap downwelling. The NOGWD completely compensates for the missing OGWD, but the compensation by a different kind of drag leads to the modification of the basic state and therefore affects the resolved wave breaking, in this case increasing the resolved wave drag.

6 Semi-annual and quasi-biennial oscillations

Given that the realistic representation of the QBO in the stratosphere may be important for seasonal predictability in the troposphere (e.g. Marshall & Scaife 2009, Butler et al. 2016), it is of interest to consider the influence of model changes on the QBO. Recall that the QBO is a quasi-periodic oscillation of the equatorial zonal wind between easterlies and westerlies in the tropical stratosphere, between 10 hPa and 100 hPa, with a mean period of 27 to 29 months. For the seasonal forecasting system SEAS4 at the ECMWF, NOGWD is tuned to produce the QBO that best agrees with the observations. For example, the amount of reduction of NOGWD flux amplitude in the tropics and the amplitude of the launch flux is different in the seasonal setting than in the medium-range setting (e.g., in seasonal forecasts on the TL grid, NOGWD flux is reduced to 40% in the tropics, whereas for medium-range forecasts the same number is 75%). In the new seasonal forecasting system SEAS5 all NOGWD parameters are the same as in the medium-range and monthly forecasting systems with cycle 45R1.

Moreover, as mentioned in the introduction, the operational high resolution (TCo1279) analysis in cycle CY41R2 develops an unphysically strong westerly phase of the SAO in the equatorial mesosphere. The zonal wind from operational analysis before and after this problem is shown in Fig. 23. The westerly wind at the equator at 0.1 hPa attains $\sim$160 m s^{-1} in May 2017 (see panels b,d and f). This magnitude is significantly stronger than the observed magnitude of $\sim$40 m s^{-1} (e.g., see Fig. 6 in Jackson et al. (1998) or Fig. 9 in Garcia et al. (1997) for equatorial zonal wind observations with the High-Resolution Doppler Imager). It is hence of interest to establish if this problem can be reproduced in the free-running model at lower resolution with different model setups. Recall that the SAO is a periodic oscillation of the equatorial zonal wind between easterlies and westerlies in the tropical mesosphere, between 0.001 hPa and 0.1 hPa, with a period of six months.

Figures 24a-f show pressure-time cross sections of equatorial zonal wind for one four-year free-running model run with different setups. To highlight the impact of modelling choices on the QBO and the SAO,

Figs. 24g-h show the time series of the equatorial zonal wind at 30 hPa and at 0.2 hPa, respectively. While the phases of the SAO and the QBO are different for forecasts initialized at other dates, the basic sensitivity to modelling choices is unchanged (not shown). It should be noted that the control run simulates a reasonably realistic QBO albeit in the model the QBO westerly phase is weaker (compare Fig. 23c with Fig. 24a between 10 and 100 hPa).

It is clear that the NOGWD has a large impact on the equatorial zonal winds and that it is the main parameterization to tune to obtain the QBO that best agrees with the observations. This was also discussed in Orr et al. (2010). Firstly, reducing NOGWD flux increases the amplitude of the easterly phase of the SAO (the maximum easterlies in the equatorial mesosphere have values of 100 m s^{-1} in the control run, 75 m s^{-1} in the increased NOGWD run, and 160 m s^{-1} in the decreased NOGWD run) and nearly kills off the westerly phases of the SAO as there is then not enough parameterized drag to drive it. The westerly phase of the SAO is too weak in the control run (maximum amplitude of 7 m s^{-1} between 0.01 and 0.1 hPa), which in the observations attains a maximum value of 40 m s^{-1} (see Fig. 6 in Jackson et al. (1998) or Fig. 9 in Garcia et al. (1997)). This can be rectified by increasing the NOGWD flux amplitude in the tropics.

Because at TL255 resolution with the default sponge specification, $\sim$60% of the westerly phase of the SAO is driven by the NOGWD, with the rest being driven by the resolved waves, the sensitivity to NOGWD is not surprising. As is shown below, the influence of the resolved waves is suppressed by the deep sponge applied from 10 hPa upwards. When the NOGWD is increased by 3.75 times, the maximum amplitude of the westerly phase of the SAO goes up to 25 m s^{-1} in Fig. 24b. When the NOGWD is decreased by 3.75 times, the maximum amplitude of the westerly phase of the SAO goes down to 4 m s^{-1} in Fig. 24c, apart from during the easterly phase of the QBO when the westerly phase of the SAO reaches amplitude of 20 m s^{-1} despite the very weak NOGWD. This westerly phase is likely driven by the resolved waves that are not filtered out by the easterly winds in the stratosphere.

The frequency of the QBO is also sensitive to the magnitude of the NOGWD (cf. panels a and b and black, blue and green lines in panel g). The phase speed increases by about three times when the NOGWD flux is increased by 3.75 times from the control value and the equatorial winds undergo what looks more like an annual oscillation than a QBO. The QBO amplitude sensitivity to NOGWD is modest, with an increase in westerly amplitude of $\sim$3 m s^{-1} when the NOGWD is increased and a decrease of westerly amplitude of $\sim$2 m s^{-1} when the NOGWD is reduced.

Interestingly, the higher grid-point resolution TCo grid coupled to the SPPT scheme has a large impact on the QBO. Firstly, it doubles the magnitude of the westerly phase and the phase speed of the QBO (cf. panels a and d). The QBO period reflects the amplitude of the wave forcing. Thus the effect of TCo+SPPT on the QBO is likely due to more eastward propagating equatorial waves present in the higher grid-point resolution TCo+SPPT run. The stronger waves can be seen in the Wheeler-Kiladis diagram of the equatorial temperature at 10 hPa in Fig. 25. There is more power in the eastward propagating equatorial Kelvin and inertia-gravity waves in the TCo+SPPT run. Because of the sensitivity of the QBO to TCo+SPPT, the tuning of the NOGWD has to be adjusted when moving from the TL to TCo grid with SPPT switched on. The westerly amplitude of the SAO also goes up to 20 m s^{-1} when the TCo grid and SPPT are used.

The removal of the sponge has a profound impact on the westerly phase of the SAO, in this case increasing the magnitude to up to 100 m s^{-1} (see cyan line in Fig. 24h). The largest increase is during the easterly QBO phase when the easterly stratospheric winds allow more resolved eastward phase speed waves to pass through without being filtered. The "no sponge" run highlights the dissipative nature of the sponge. Therefore, the model at TL255 resolution is perfectly capable of simulating the westerly phase

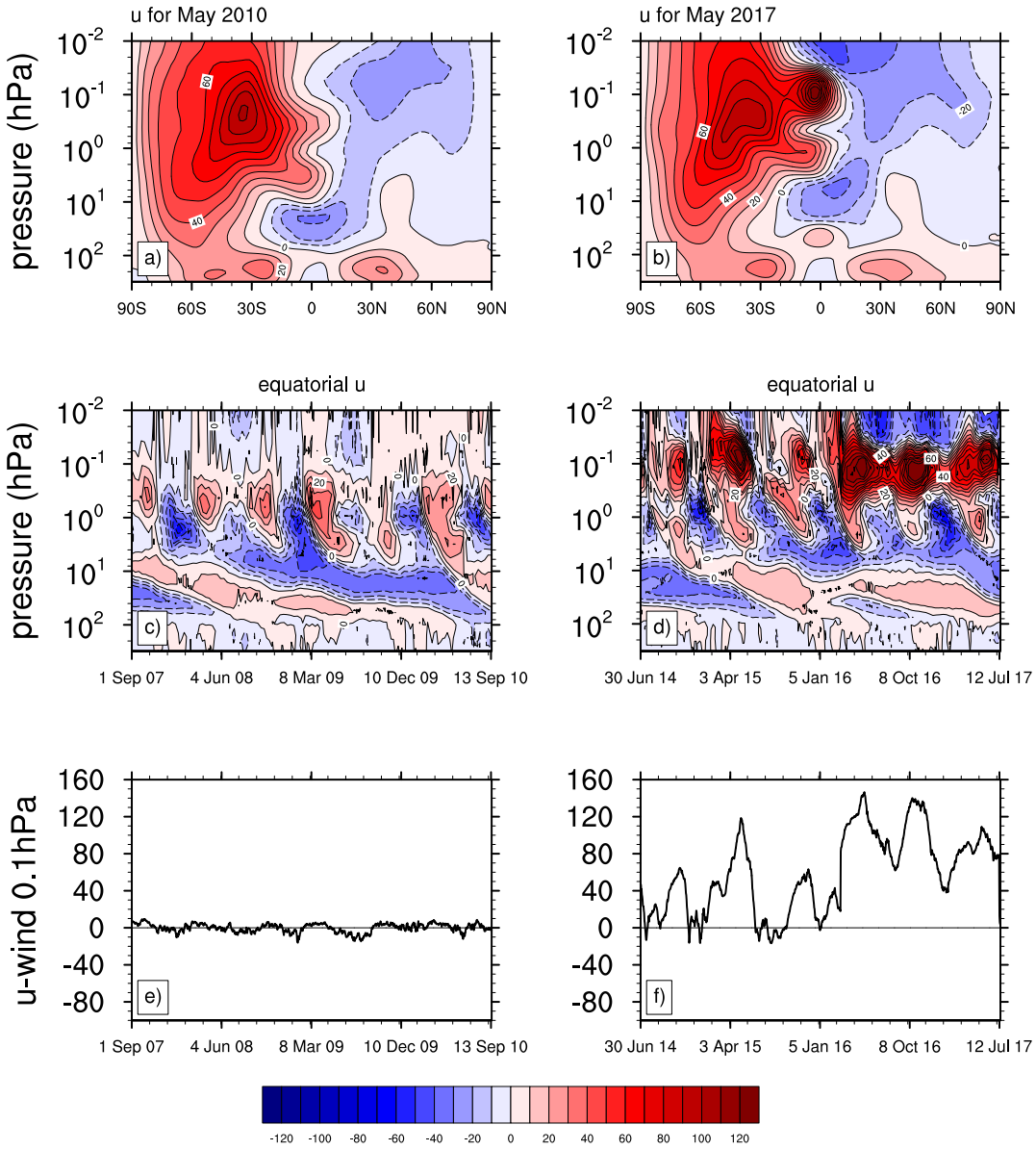

Figure 23: (a)-(b): Zonal mean zonal wind for May (a) 2010 and (b) 2017 from the operational analysis. (c)-(d) Pressure-time cross sections of equatorial zonal winds (averaged in latitude between ±5 °N/S) for three years of the analysis for (c) Sept 2007 to Sept 2010 and (d) June 2014 to June 2017. (e)-(f): Time series of equatorial zonal wind at 0.1 hPa for (e) Sept 2007 to Sept 2010 and (f) June 2014 to June 2017. Contour interval in panels a-d is 10 m s^{-1}.

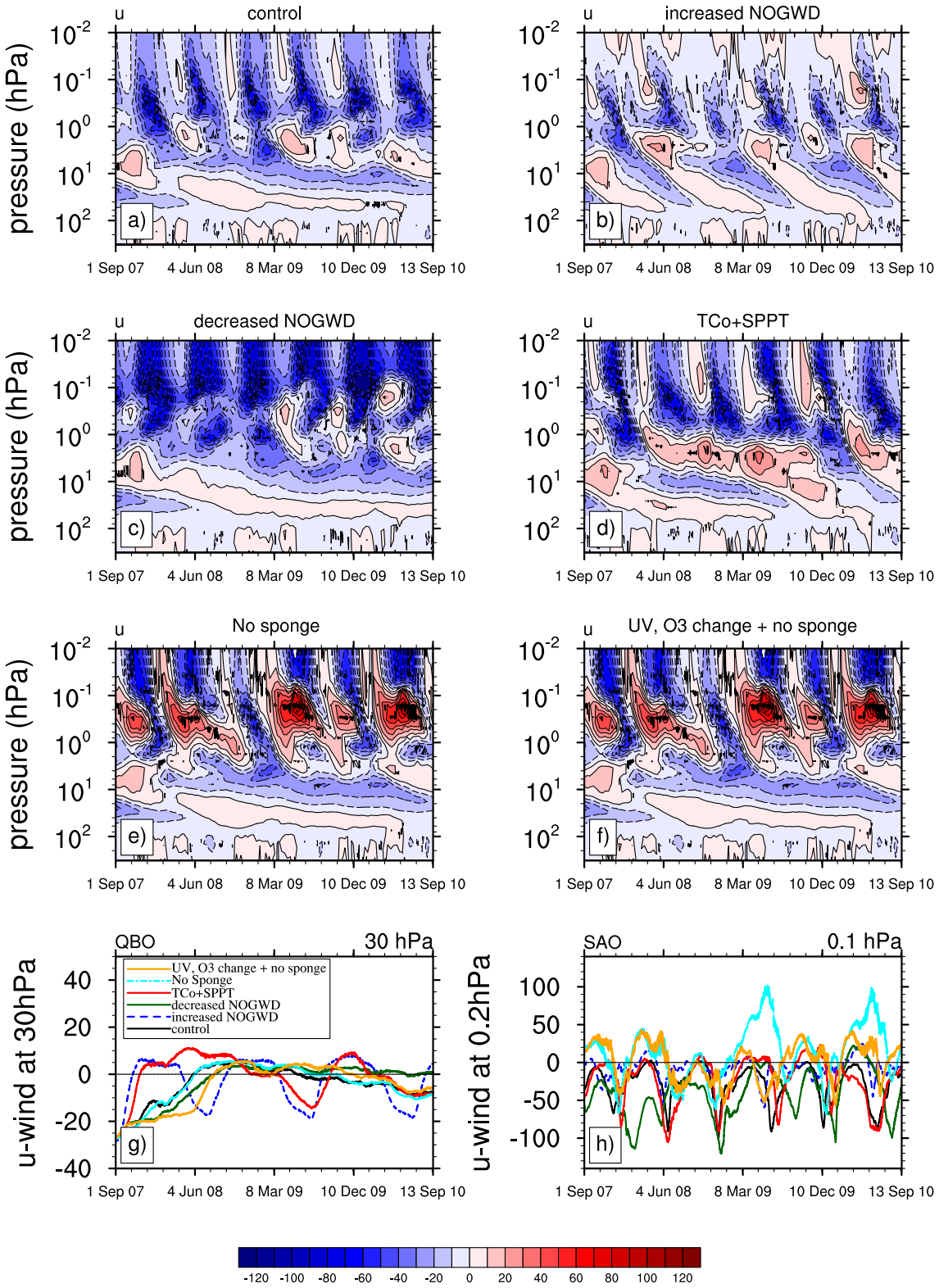

Figure 24: (a)-(f): Pressure-time cross sections of equatorial zonal winds (averaged in latitude between ±5 °N/S) for one four-year forecast of the free-running model. (a) The control run; (b) increased NOGWD run; (c) decreased NOGWD run; (d) TCo + SPPT; (e) no sponge; (f) reduced UV absorption, diurnal cycle of ozone + no sponge. (g)-(h): Time series of equatorial zonal wind at (g) 30 hPa to indicate QBO behaviour and at (h) 0.2 hPa to indicate SAO behaviour for the runs in panels a-f.

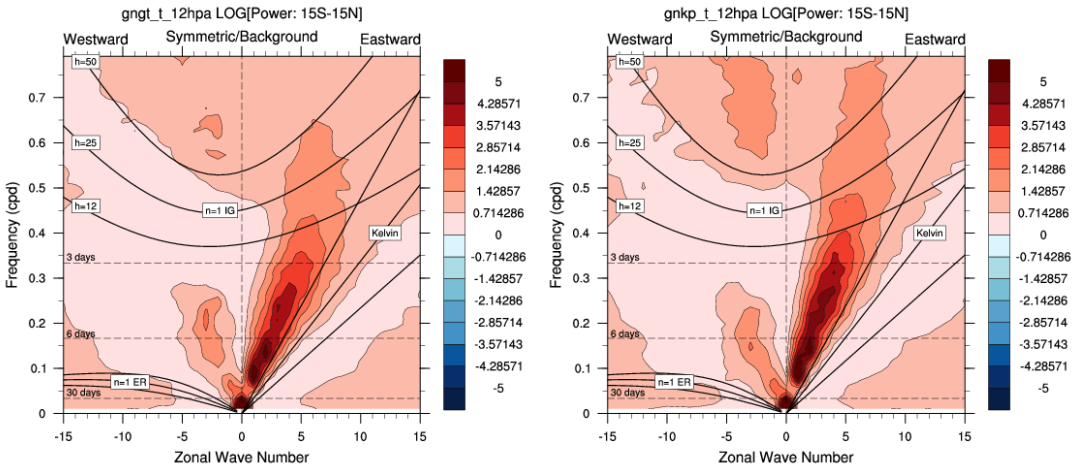

Figure 25: Wheeler-Kiladis diagram of the symmetric background spectrum of temperature at 10 hPa for the control run (left) and the TCo+SPPT run (right). Note more power in the eastward propagating waves in the TCo+SPPT run.

of the SAO without NOGWD. If anything, the resolved eastward phase speed waves are too active in the mesosphere in the absence of a sponge. However, the sponge appears to have a negligible influence on the QBO (cf. cyan and black lines in panel g).

Similar behaviour of equatorial zonal winds with model changes can also be seen in the nudged setup 2. Figs. 26 and 27 show pressure-time cross sections of equatorial zonal winds for the nudged setup where two six month seasonal forecasts are concatenated together. This figure also includes the "no OGWD" experiment, which shows that OGWD has no influence on the SAO or the QBO.

6.1 Section summary

- NOGWD has a large impact on the QBO and the SAO at T255L137 resolution. The easterly phase of the SAO is enhanced with the reduction in NOGWD flux. The amplitude of the westerly phase of the SAO and the QBO and the frequency of the QBO is increased with increase in NOGWD.
- The use of TCo+SPPT increases the frequency and the amplitude of the westerly phase of the QBO by a factor of two from the control run.
- Switching off the sponge enhances the westerly phase of the SAO by 15 times, but does not affect the QBO. Therefore a lack of sponge can lead to strong mesospheric westerly winds at the equator.
- The inclusion of the diurnal cycle of ozone and the reduction in solar UV absorption has little impact on the SAO and the QBO. The same is true for OGWD in the middle atmosphere.

7 Conclusions, actions and open questions

This report focused on the middle atmosphere circulation and its sensitivity to model changes in free-running and nudged model at T255L137 resolution. It is important to stress that at this resolution a

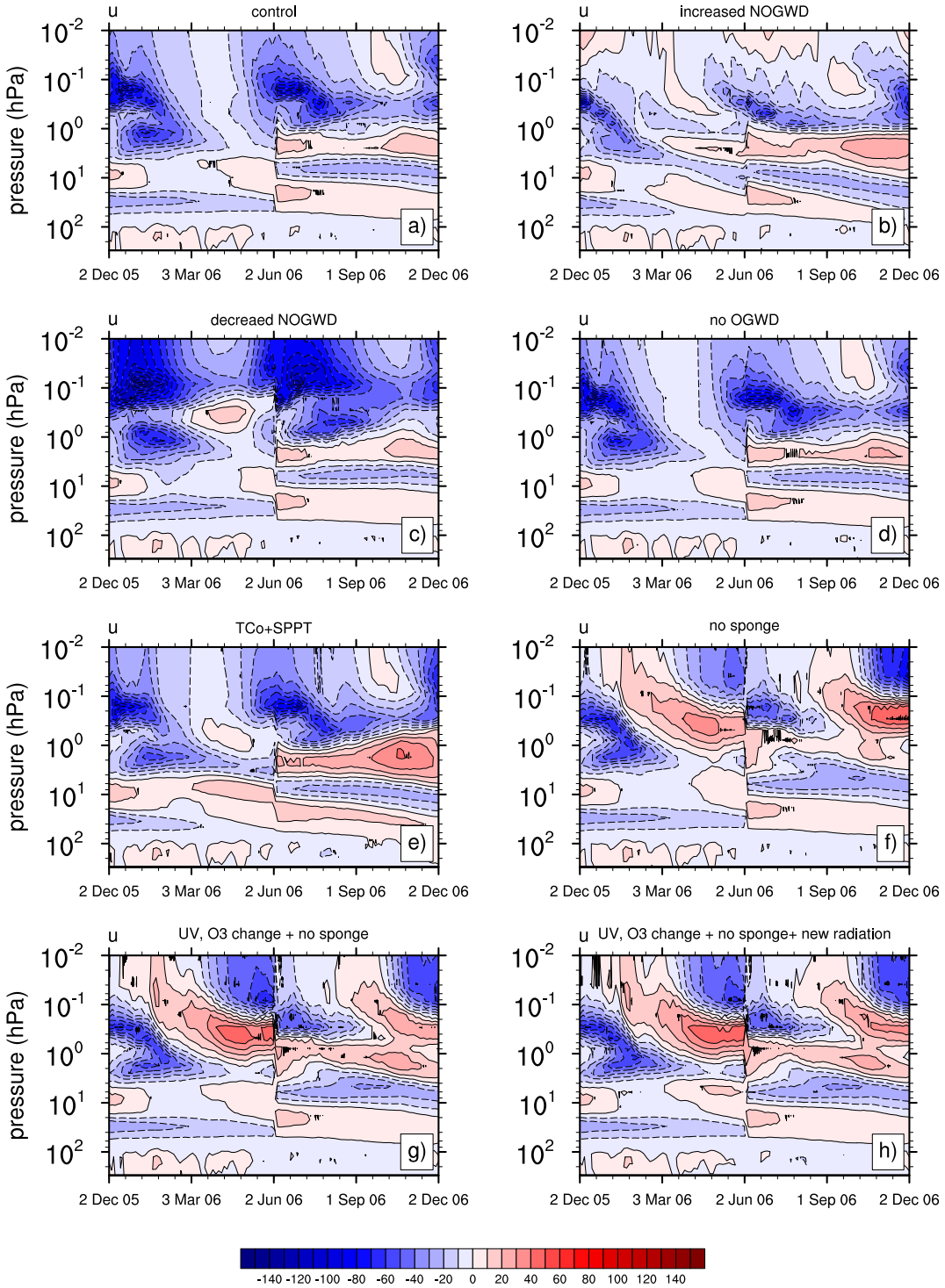

Figure 26: Pressure-time cross sections of the equatorial zonal winds (averaged in latitude between ±5 °N/S) for the nudged model. (a) The control run; (b) increased NOGWD run; (c) decreased NOGWD run; (d) no OGWD; (e) TCo + SPPT; (f) no sponge; (g) reduced UV absorption, diurnal cycle of ozone + no sponge; (h) as (g) but with the new radiation scheme. The nudged forecasts are concatenated together on the 01/06/2006.

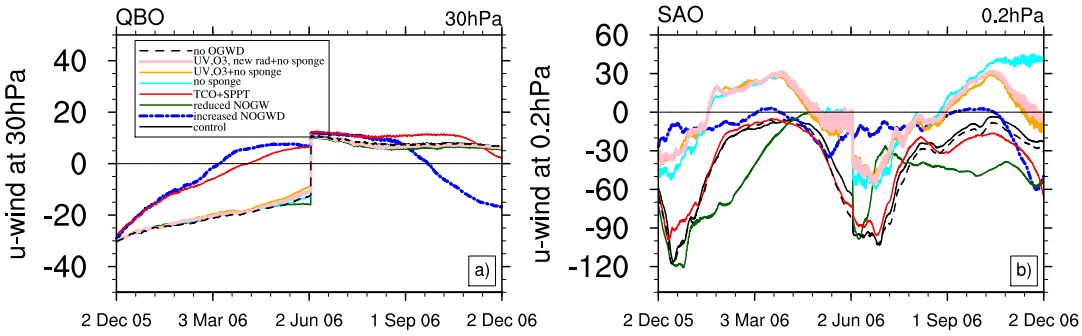

Figure 27: Time series of equatorial zonal wind at (a) 30 hPa and at (b) 0.2 hPa for the simulations shown in Fig. 26. The control run curve in (a) is identical to the "UV,O3,new rad+no sponge" curve.

substantial part of inertia-gravity wave activity is not resolved. While the key findings are summarized at the end of each results section, some implications and conclusions from this work are now considered.

- The main finding is that the NOGWD exerts a strong influence on the middle atmosphere circulation at T255 resolution, especially in the SH where the contribution of the NOGWD to the residual mean meridional circulation is larger than in the NH. Therefore NOGWD is the dominant parameterization to tune for the middle atmosphere circulation, as it affects the BDC strength, the QBO and the SAO amplitudes, and the QBO frequency in both the free-running and the nudged runs. While the BDC strength is not directly observed, the BDC influences temperature distribution and therefore the tuning should be done against seasonal temperature biases. The amplitude of NOGWD flux in the tropics controls the QBO and the SAO, whereas the amplitude of the NOGWD flux in the extra-tropics controls the polar cap downwelling strength and hence the temperature and the zonal wind distributions in the extra-tropics. Hence, NOGWD flux amplitude is the main parameter to tune in the parametrization to get the QBO and the seasonal polar stratospheric temperature right, both of which are important for tropospheric predictability. The SAO exerts little impact on the stratosphere and is not believed to be important for tropospheric predictability. Therefore it is not important to accurately model the SAO, only to ensure that the SAO amplitude does not get too large for model stability, nor adversely influence assimilated observations in the stratosphere, given the deep weighting functions of the operational temperature sounders. It should be emphasized, however, that the current NOGWD settings seem optimal for the seasonal temperature and zonal wind distributions off the equator in cycle 43R1. This might not be the case at higher resolution or might change when new numerics and physics updates are introduced in future model cycles.

- The amplitude of the specified NOGWD flux strongly affects the polar temperatures, which are tied to the response in the residual mean meridional circulation. In the absence of the resolved wave drag and OGWD in the summer hemisphere, the summer pole temperatures change in proportion with NOGWD flux changes with cooling occurring in response to increase in NOGWD flux and warming in response to decrease in NOGWD flux.

- In the winter hemisphere, the interaction with the resolved waves complicates the interpretation of the BDC response to changes in NOGWD. Generally, in response to increased NOGWD the resolved wave forcing decreases in the polar mid- to upper-stratosphere and increases in the polar lower stratosphere due to a weakened polar night jet that is more susceptible to wave breaking. Whether the overall strength of the polar cap downwelling in the stratosphere decreases or in-

creases in response to increase in NOGWD depends on the partitioning of the resolved and parameterized waves in driving the downwelling. An increase in NOGWD increases the downwelling in the SH but decreases the downwelling in the NH. Moreover, there appears to be a seasonal offset in the interaction between the resolved and parameterized waves that is larger in the SH. Therefore, during early winter the downwelling changes are almost proportional to changes in NOGWD whereas in the late winter/early spring the resolved wave changes, brought about by changes to NOGWD, dominate the response. Thus the seasonal mean perspective might paint a misleading picture of the resolved and parameterized wave interaction. In the NH, the interaction with the OGWD further complicates the matter. Therefore, it is unlikely that NOGWD and OGWD can be tuned independently at the explored resolution. However, at high horizontal resolution, such as TCo1279, independent tuning may become feasible as OGWD is small.

- NOGWD amplitude impacts the QBO and the SAO with the increase in flux resulting in an increase in the westerly phase amplitude of the SAO and the QBO and an increase in the QBO frequency. Because the QBO amplitude and frequency also increases with the use of TCo+SPPT, NOGWD has to be re-tuned when moving from the linear to the TCo grid. Whether the QBO changes are mainly driven by the SPPT scheme, the TCo grid or both remains to be established.

- The strong dependence on NOGWD found here is likely to be lessened at horizontal resolution higher than 29 km because the specified NOGWD flux decreases below 29 km and vanishes completely at 1 km in IFS. Therefore for high horizontal resolutions the role of NOGWD in driving BDC, SAO and QBO should decrease and the response for relative parametrized flux changes is expected to be lower. Apart from the horizontal resolution dependence built into the non-orographic parametrization scheme, the role of resolved gravity waves is expected to increase at higher horizontal resolution. This might lead to a decrease in parametrized drag due to compensating effects at horizontal resolutions lower than 29 km. Moreover, the resolved gravity waves may be sensitive to model numerics making model "tuning" more difficult.

- The sponge clearly affects the amplitude of the westerly phase of the SAO. Without the damping effect of the sponge, the waves in the model are well resolved to simulate the SAO though the amplitude of the wave forcing is stronger than in the observations.

- Even in the absence of a sponge the mesospheric equatorial zonal winds do not reach 160 m/s in the free-running model at T255 spectral truncation. Therefore, the free-running model is unable to reproduce the "mesospheric jet problem" at this resolution. Note, that tests carried out with the free-running model at TL639L139 resolution also lacked such strong equatorial westerlies.

- The current sponge formulation which applies more damping on the divergence and dissipates the mean flow, tends to globally warm the mesosphere. The radiation changes coupled to a sponge that does not dissipate the mean flow and that applies an equal amount of damping on the rotational and divergent flow would almost eliminate the global mesospheric warm bias. However, neither of these changes eliminate the persistent mid- to high-latitude warm bias present in the SH winter stratosphere, or the cold summer tropopause bias.

- The nudged framework is powerful in understanding the middle atmosphere circulation response to model changes that impact the middle atmosphere only, such as NOGWD. As the tropospheric variability is eliminated in the nudged framework, it is cheaper to obtain statistically significant results.

- The nudged framework allows for an investigation of the impact of OGWD on the middle atmosphere circulation as the troposphere is not adversely affected by the removal of OGWD. As

expected from the dominance of the OGWD in the NH, the removal of OGWD has the largest impact there. The absence of OGWD is completely compensated by NOGWD. This compensation affects the background flow leading to increased resolved wave breaking and strengthening of the polar cap downwelling. Hence, the interaction of the two types of parametrized drag with the resolved wave drag in the NH can lead to unexpected circulation changes.

- The higher grid-point resolution TCo grid coupled to SPPT has a similar magnitude impact on the tropical upwelling in the lower stratosphere as the NOGWD changes in both the free-running and the nudged setups. In particular, there is an increase in the upwelling that is associated with $\sim$ 1-2 K cooling in the lowermost stratosphere. Both the increase in upwelling and the stronger QBO amplitude and frequency support the hypothesis of more resolved wave forcing with the use of TCo+SPPT. The impact of the TCo+SPPT on the polar cap downwelling is less clear and depends on the experimental framework.
- It is unlikely that the persistent high latitude upper-stratospheric warm bias in the SH winter and the tropical lower stratospheric cold bias are a result of too strong a residual mean meridional circulation.
- As already reported in ECMWF (2017), the reduction in the solar UV and the inclusion of the approximate diurnal cycle of ozone in the middle atmosphere greatly reduces the global warm mesospheric bias and somewhat reduces the SH winter high latitude warm bias in the upper stratosphere. However, the radiation changes have little impact on the BDC or on the QBO and the SAO. This is likely due to the temperature gradients not being greatly affected by the radiation changes.
- The tropical tape recorder signal is unaffected by any of the model changes explored here.

Actions:

- Given that the QBO and the SAO behave differently in the TL255 and TCo255+SPPT runs, NOGWD tuning should be performed using the TCo grid, as it is used operationally.
- The application of the sponge on the zonal mean fields (i.e., zonal wavenumber $m = 0$ modes in the spherical harmonic expansion) should be removed. There should be only one sponge which will apply an equal amount of damping on the rotational and divergent modes.
- Once the new sponge has been developed, NOGWD needs to be returned (with the use of TCo grid) to provide a middle-atmosphere circulation that best agrees with the observations.

Open questions:

1. Do all conclusions in this report hold at the operational resolution of TCo1279?
2. Given its importance, how can we tune NOGWD with every model cycle in a semi-automatic way based on observations (e.g., the long-lived tracers)?
3. None of the model changes eradicated the persistent mid- to high-latitude SH winter warm bias. Is this bias of radiative origin (e.g., including the sphericity effect in solar heating might be important for the middle-atmosphere (Fomichev et al. 2004))?
4. What is the impact of model changes on the persistence of SSWs and the downward propagation of the stratospheric signal in the free-running IFS?

5. NH winter 2005/2006 experienced a long-lived SSW event, which is believed to be important for tropospheric predictability. The impact of model changes on such long-lived SSW events can be studied using the nudged framework.

6. Analysis of the ERA-I data shows that the date of the SH vortex breakup (i.e., the final warming date) has an impact on tropospheric variability Byrne et al. (2017). Does this stratosphere-troposphere coupling occur in the free-running IFS?

7. Climate models have a late bias in the breakup of the SH vortex (see figure 14 in (Butchart et al. 2011)). How well is the vortex breakup date captured in the free-running model and how do the model changes impact the breakup date?

8. Is the reduction in upwelling inferred from the tropical tape recorder signal between ERA-I and the free-running model due to changes in the vertical and horizontal resolutions? The fact that the tape recorder signal in ERA-5 (which has higher horizontal and vertical resolution than ERA-I) is similar to the signal in the free-running model may indicate that the vertical and horizontal resolutions are important.

9. Are some distributions of vertical levels significantly better in representing the stratospheric circulation?

10. Is the circulation response seen here in response to TCo+SPPT mainly due to the higher grid-point resolution TCo grid, the SPPT scheme, or both?

11. What impact does the NOGWD launch level have on the tropical upwelling? If the launch level is moved higher up, outside the troposphere, does the tropical upwelling sensitivity to NOGWD disappear?

12. What impact does introducing intermittency and source dependency to NOGWD parametrization (e.g., de la Cmara et al. 2016) have on the middle atmosphere circulation?

Acknowledgments

The authors thank Irina Sandu and Nils Wedi for providing support to carry out this project and for useful comments on the manuscript. Peter Hitchcock is thanked for providing gridded MLS temperature data.

References

Andrews, D. G., Holton, J. R. & Leovy, C. B. (1987), *Middle atmosphere dynamics*, number 40, Academic press.

Baldwin, M. P. & Dunkerton, T. J. (2001), 'Stratospheric harbingers of anomalous weather regimes', *Science* **294**(5542), 581–584.

Black, R. X. & McDaniel, B. A. (2007), 'Interannual variability in the southern hemisphere circulation organized by stratospheric final warming events', *Journal of the atmospheric sciences* **64**(8), 2968–2974.

Boer, G., Arpe, K., Blackburn, M., Déqué, M., Gates, W., Hart, T., Le Treut, H., Rorteckner, E., Sheinin, D., Simmonds, I. et al. (1992), 'Some results from an intercomparison of the climates simulated by 14 atmospheric general circulation models', *Journal of Geophysical Research: Atmospheres* **97**(D12), 12771–12786.

Butchart, N. (2014), 'The Brewer-Dobson circulation', *Reviews of Geophysics* **52**(2), 157–184.

Butchart, N., Charlton-Perez, A. J., Cionni, I., Hardiman, S., Haynes, P., Krüger, K., Kushner, P., Newman, P., Osprey, S., Perlwitz, J. et al. (2011), 'Multimodel climate and variability of the stratosphere', *Journal of Geophysical Research: Atmospheres* **116**(D5).

Butler, A. H., Arribas, A., Athanassiadou, M., Baehr, J., Calvo, N., Charlton-Perez, A., Dqu, M., Domeisen, D. I. V., Frhlich, K., Hendon, H., Imada, Y., Ishii, M., Iza, M., Karpechko, A. Y., Kumar, A., MacLachlan, C., Merryfield, W. J., Mller, W. A., O'Neill, A., Scaife, A. A., Scinocca, J., Sigmond, M., Stockdale, T. N. & Yasuda, T. (2016), 'The climate-system historical forecast project: do stratosphere-resolving models make better seasonal climate predictions in boreal winter?', *Quarterly Journal of the Royal Meteorological Society* **142**(696), 1413–1427.

Byrne, N. J., Shepherd, T. G., Woollings, T. & Plumb, R. A. (2017), 'Nonstationarity in southern hemisphere climate variability associated with the seasonal breakdown of the stratospheric polar vortex', *Journal of Climate* **30**(18), 7125–7139.

Charney, J. G. & Drazin, P. G. (1961), 'Propagation of planetary-scale disturbances from the lower into the upper atmosphere', *Journal of Geophysical Research* **66**(1), 83–109.

Chen, C.-C. & Rasch, P. J. (2012), 'Climate simulations with an isentropic finite-volume dynamical core', *Journal of Climate* **25**(8), 2843–2861.

de la Cmara, A., Lott, F. & Abalos, M. (2016), 'Climatology of the middle atmosphere in lmdz: Impact of source-related parameterizations of gravity wave drag', *Journal of Advances in Modeling Earth Systems* **8**(4), 1507–1525.

Dee, D., Uppala, S., Simmons, A., Berrisford, P., Poli, P., Kobayashi, S., Andrae, U., Balmaseda, M., Balsamo, G., Bauer, P., Bechtold, P., Beljaars, A., van de Berg, L., Bidlot, J., Bormann, N., Delsol, C., Dragani, R., Fuentes, M., Geer, A., Haimberger, L., Healy, S., Hersbach, H., Holm, E., Isaksen, L., Kallberg, P., Kohler, M., Matricardi, M., McNally, A., Monge-Sanz, B., Morcrette, J., Park, B., Peubey, C., de Rosnay, P., Tavolato, C., Thepaut, J. & Vitart, F. (2011), 'The era-interim reanalysis: Configuration and performance of the data assimilation system', *Quarterly Journal of the royal meteorological society* **137**(656), 553–597.

Diamantakis, M. (2013), 'The semi-lagrangian technique in atmospheric modelling: current status and future challenges'.

Douville, H. (2009), 'Stratospheric polar vortex influence on northern hemisphere winter climate variability', *Geophysical Research Letters* **36**(18), n/a–n/a. L18703.

Dunkerton, T. J. (1997), 'The role of gravity waves in the quasi-biennial oscillation', *Journal of Geophysical Research: Atmospheres* **102**(D22), 26053–26076.

ECMWF (2016), 'IFS documentation. CY43R1', *http://www.ecmwf.int/en/forecasts/documentation-and-support/changes-ecmwf-model/ifs-documentation.* .

ECMWF (2017), Radiation in numerical weather prediction, Technical report, Special Topic Paper,ECMWF.

Fomichev, V. I., Fu, C., de Grandpr, J., Beagley, S. R., Ogibalov, V. P. & McConnell, J. C. (2004), 'Model thermal response to minor radiative energy sources and sinks in the middle atmosphere', *Journal of Geophysical Research: Atmospheres* **109**(D19), n/a–n/a. D19107.

Fritts, D. C. & Alexander, M. J. (2003), 'Gravity wave dynamics and effects in the middle atmosphere', *Reviews of Geophysics* **41**(1), n/a–n/a. 1003.

Garcia, R. R., Dunkerton, T. J., Lieberman, R. S. & Vincent, R. A. (1997), 'Climatology of the semiannual oscillation of the tropical middle atmosphere', *Journal of Geophysical Research: Atmospheres* **102**(D22), 26019–26032.

Geller, M. A., Alexander, M. J., Love, P. T., Bacmeister, J., Ern, M., Hertzog, A., Manzini, E., Preusse, P., Sato, K., Scaife, A. A. & Zhou, T. (2013), 'A comparison between gravity wave momentum fluxes in observations and climate models', *Journal of Climate* **26**(17), 6383–6405.

Glanville, A. A. & Birner, T. (2017), 'Role of vertical and horizontal mixing in the tape recorder signal near the tropical tropopause', *Atmospheric Chemistry and Physics* **17**(6), 4337–4353.

Haynes, P. H., McIntyre, M. E., Marks, C. J., Shepherd, T. G. & Shine, K. P. (1991), 'On the "downward control" of extratropical diabatic circulations by eddy-induced mean zonal forces', *Journal of the Atmospheric Sciences* **48**(4), 651–678.

Holton, J. (1990), 'On the global exchange of mass between the stratosphere and troposphere', *Journal of the atmospheric sciences* **47**(3), 392–395.

Jackson, D. R., Burrage, M. D., Harries, J. E., Gray, L. J. & Russell, J. M. (1998), 'The semi-annual oscillation in upper stratospheric and mesospheric water vapour as observed by haloe', *Quarterly Journal of the Royal Meteorological Society* **124**(551), 2493–2515.

Kushner, P. J. & Polvani, L. M. (2004), 'Stratosphere–troposphere coupling in a relatively simple agcm: The role of eddies', *Journal of climate* **17**(3), 629–639.

Livesey, N. J., Read, W. G., Froidevaux, L., Lambert, A., Manney, G. L., Pumphrey, H. C., Santee, M. L., Schwartz, M. J., Wang, S., Cofield, R. E. et al. (2011), 'Version 3.3 level 2 data quality and description document', *JPL D-33509* .

Lott, F. & Miller, M. J. (1997), 'A new subgrid-scale orographic drag parametrization: Its formulation and testing', *Quarterly Journal of the Royal Meteorological Society* **123**(537), 101–127.

Malardel, S., Wedi, N., Deconinck, W., Diamantakis, M., Kühnlein, C., Mozdzynski, G., Hamrud, M. & Smolarkiewicz, P. (2016), 'A new grid for the IFS', *ECMWF Newsl* **146**, 23–28.

Marshall, A. G. & Scaife, A. A. (2009), 'Impact of the qbo on surface winter climate', *Journal of Geophysical Research: Atmospheres* **114**(D18).

McLandress, C. & Shepherd, T. G. (2009), 'Simulated anthropogenic changes in the Brewer-Dobson circulation, including its extension to high latitudes', *Journal of Climate* **22**(6), 1516–1540.

McLandress, C., Shepherd, T. G., Polavarapu, S. & Beagley, S. R. (2012), 'Is missing orographic gravity wave drag near 60 °S the cause of the stratospheric zonal wind biases in chemistry–climate models?', *Journal of the Atmospheric Sciences* **69**(3), 802–818.

Meyer, W. D. (1970), 'A diagnostic numerical study of the semiannual variation of the zonal wind in the tropical stratosphere and mesosphere', *Journal of the Atmospheric Sciences* **27**(5), 820–830.

Mote, P. W., Dunkerton, T. J., McIntyre, M. E., Ray, E. A., Haynes, P. H. & Russell, J. M. (1998), 'Vertical velocity, vertical diffusion, and dilution by midlatitude air in the tropical lower stratosphere', *Journal of Geophysical Research: Atmospheres* **103**(D8), 8651–8666.

Mote, P. W., Rosenlof, K. H., McIntyre, M. E., Carr, E. S., Gille, J. C., Holton, J. R., Kinnersley, J. S., Pumphrey, H. C., Russell III, J. M. & Waters, J. W. (1996), 'An atmospheric tape recorder: The imprint of tropical tropopause temperatures on stratospheric water vapor'.

Orr, A., Bechtold, P., Scinocca, J., Ern, M. & Janiskova, M. (2010), 'Improved middle atmosphere climate and forecasts in the ECMWF model through a nonorographic gravity wave drag parameterization', *Journal of Climate* **23**(22), 5905–5926.

Palmer, T., Buizza, R., Doblas-Reyes, F., Jung, T., Leutbecher, M., Shutts, G., Steinheimer, M. & Weisheimer, A. (2009), 'Stochastic parametrization and model uncertainty', *ECMWF Tech. Memo* **598**, 1–42.

Plougonven, R. & Zhang, F. (2014), 'Internal gravity waves from atmospheric jets and fronts', *Reviews of Geophysics* **52**(1), 33–76.

Plumb, R. A. (2002), 'Stratospheric transport', *Journal of the Meteorological Society of Japan. Ser. II* **80**(4B), 793–809.

Pope, V., Pamment, J., Jackson, D. & Slingo, A. (2001), 'The representation of water vapor and its dependence on vertical resolution in the hadley centre climate model', *Journal of climate* **14**(14), 3065–3085.

Pulido, M. & Thuburn, J. (2008), 'The seasonal cycle of gravity wave drag in the middle atmosphere', *Journal of Climate* **21**(18), 4664–4679.

Quintanar, A. I. & Mechoso, C. R. (1995), 'Quasi-stationary waves in the southern hemisphere. part i: Observational data', *Journal of climate* **8**(11), 2659–2672.

Randel, W. J. (1988), 'The seasonal evolution of planetary waves in the southern hemisphere stratosphere and troposphere', *Quarterly Journal of the Royal Meteorological Society* **114**(484), 1385–1409.

Randel, W. J., Garcia, R. & Wu, F. (2008), 'Dynamical balances and tropical stratospheric upwelling', *Journal of the Atmospheric Sciences* **65**(11), 3584–3595.

Ray, E. A., Alexander, M. J. & Holton, J. R. (1998), 'An analysis of the structure and forcing of the equatorial semiannual oscillation in zonal wind', *Journal of Geophysical Research: Atmospheres* **103**(D2), 1759–1774.

Sakazaki, T., Sasaki, T., Shiotani, M., Tomikawa, Y. & Kinnison, D. (2015), 'Zonally uniform tidal oscillations in the tropical stratosphere', *Geophysical Research Letters* **42**(21), 9553–9560.

Sato, K. & Dunkerton, T. J. (1997), 'Estimates of momentum flux associated with equatorial kelvin and gravity waves', *Journal of Geophysical Research: Atmospheres* **102**(D22), 26247–26261.

Scheffler, G. & Pulido, M. (2017), 'Estimation of gravity-wave parameters to alleviate the delay in the antarctic vortex breakup in general circulation models', *Quarterly Journal of the Royal Meteorological Society* **143**(706), 2157–2167.

Scinocca, J. F. (2003), 'An accurate spectral nonorographic gravity wave drag parameterization for general circulation models', *Journal of the atmospheric sciences* **60**(4), 667–682.

Seviour, W. J., Butchart, N. & Hardiman, S. C. (2012), 'The Brewer–Dobson circulation inferred from era-interim', *Quarterly Journal of the Royal Meteorological Society* **138**(665), 878–888.

Shaw, T. A., Sigmond, M., Shepherd, T. G. & Scinocca, J. F. (2009), 'Sensitivity of simulated climate to conservation of momentum in gravity wave drag parameterization', *Journal of Climate* **22**(10), 2726–2742.

Shepherd, T. G. (2000), 'The middle atmosphere', *Journal of Atmospheric and Solar-Terrestrial Physics* **62**(17), 1587–1601.

Shepherd, T. G., Semeniuk, K. & Koshyk, J. N. (1996), 'Sponge layer feedbacks in middle-atmosphere models', *Journal of Geophysical Research: Atmospheres* **101**(D18), 23447–23464.

Sigmond, M., Scinocca, J. F., Kharin, V. V. & Shepherd, T. G. (2013), 'Enhanced seasonal forecast skill following stratospheric sudden warmings', *Nature Geoscience* **6**(2), 98–102.

Sigmond, M. & Shepherd, T. G. (2014), 'Compensation between resolved wave driving and parameterized orographic gravity wave driving of the Brewer–Dobson circulation and its response to climate change', *Journal of Climate* **27**(14), 5601–5610.

SPARC CCMVal Report on the Evaluation of Chemistry-Climate Models (2010), Technical report, SPARC.